Flow and travel time statistics in highly heterogeneous porous media

Hrvoje Gotovac,[1,2] Vladimir Cvetkovic,[1] and Roko Andricevic[2]

Received 18 May 2008; revised 23 March 2009; accepted 30 April 2009; published 3 July 2009.

[1] In this paper we present flow and travel time ensemble statistics based on a new simulation methodology, the adaptive Fup Monte Carlo method (AFMCM). As a benchmark case, we considered two-dimensional steady flow in a rectangular domain characterized by multi-Gaussian heterogeneity structure with an isotropic exponential correlation and *lnK* variance σ_Y^2 up to 8. Advective transport is investigated using the travel time framework where Lagrangian variables (e.g., velocity, transverse displacement, or travel time) depend on space rather than on time. We find that Eulerian and Lagrangian velocity distributions diverge for increasing *lnK* variance due to enhanced channeling. Transverse displacement is a nonnormal for all σ_Y^2 and control planes close to the injection area, but after $xI_Y = 20$ was found to be nearly normal even for high σ_Y^2. Travel time distribution deviates from the Fickian model for large *lnK* variance and exhibits increasing skewness and a power law tail for large *lnK* variance, the slope of which decreases for increasing distance from the source; no anomalous features are found. Second moment of advective transport is analyzed with respect to the covariance of two Lagrangian velocity variables: slowness and slope which are directly related to the travel time and transverse displacement variance, which are subsequently related to the longitudinal and transverse dispersion. We provide simple estimators for the Eulerian velocity variance, travel time variance, slowness, and longitudinal dispersivity as a practical contribution of this analysis. Both two-parameter models considered (the advection-dispersion equation and the lognormal model) provide relatively poor representations of the initial part of the travel time probability density function in highly heterogeneous porous media. We identify the need for further theoretical and experimental scrutiny of early arrival times, and the need for computing higher-order moments for a more accurate characterization of the travel time probability density function. A brief discussion is presented on the challenges and extensions for which AFMCM is suggested as a suitable approach.

Citation: Gotovac, H., V. Cvetkovic, and R. Andricevic (2009), Flow and travel time statistics in highly heterogeneous porous media, *Water Resour. Res.*, *45*, W07402, doi:10.1029/2008WR007168.

1. Introduction

[2] Because of the obvious limitations and difficulties in carrying out physical experiments on transport in heterogeneous porous media, numerical simulations have always been an indispensable part of theoretical advances [*Freeze*, 1975]. First-order analysis [e.g., *Dagan*, 1982, 1984; *Shapiro and Cvetkovic*, 1988; *Rubin*, 1990] has been provided a solid basis for predictions. More recent extensions to second-order theories [*Dagan*, 1994; *Deng and Cushman*, 1995; *Hsu et al.*, 1996; *Hsu and Lamb*, 2000] have further strengthened the confidence in the analytical methods for predicting transport in heterogeneous formations. Although first- and second-order theoretical results have significantly advanced our understanding of flow and advective transport in heterogeneous porous media, and constitute indispensable predictive tools, their limitations are still not fully understood and are an ongoing topic of investigations where numerical tools play a central role [*Bellin et al.*, 1992, 1994; *Chin and Wang*, 1992; *Cvetkovic et al.*, 1996; *Salandin and Fiorotto*, 1998; *Hassan et al.*, 1998; *Maxwell et al.*, 1999; *Hassan et al.*, 2001; *Rubin*, 2003; *Janković et al.*, 2003; *de Dreuzy et al.*, 2007].

[3] On the one hand, the perturbation expansions would imply that the first-order results should strictly apply only for $\sigma_Y^2 \ll 1$. On the other hand, numerical simulations indicate that the first-order results are robust and applicable for σ_Y^2 close to and even above 1 [*Bellin et al.*, 1992; *Salandin and Fiorotto*, 1998; *Hassan et al.*, 1998]; this has been explained by a combined effect of reduced fluctuations and increased correlation of the flow field relative to the *lnK* field. Furthermore, the Lagrangian/trajectory theoretical approaches [e.g., *Dagan*, 1982, 1984; *Shapiro and Cvetkovic*, 1988] typically assume the equivalence between Lagrangian and Eulerian flow fields, the statistics of which

[1]Department of Land and Water Resources Engineering, Royal Institute of Technology (KTH), Stockholm, Sweden.
[2]Department of Civil and Architectural Engineering, University of Split, Split, Croatia.

0043-1397/09/2008WR007168$09.00

can diverge for increasing variability. Thus there are still open issues regarding the relationship between the *lnK* and Lagrangian random fields, the resolution of which can provide more reliable predictive tools.

[4] Geological formations may exhibit a wide range of heterogeneous structures, often with significant complexity depending on the scale of interest. Typical well known examples are low heterogeneous Borden ($\sigma_Y^2 = 0.29$ [*Mackay et al.*, 1986]) and Cape Cod ($\sigma_Y^2 = 0.26$ [*LeBlanc et al.*, 1991]) aquifers or highly heterogeneous Columbus aquifers (MADE-1 and MADE-2 tracer test [*Boggs et al.*, 1992]) with approximately $\sigma_Y^2 = 4.5$ consisting of, for instance, alluvial terrace deposits composed of sand and gravel with minor amounts of silt and clay which span hydraulic conductivity values over 6 orders of magnitude. Therefore variations in the hydraulic properties may be very large and it is of considerable theoretical and practical interest to better understand flow and advective transport in formations of high heterogeneity. To this end, numerical simulations are a first choice as an experimental method; however, accurate simulations of flow and advective transport in highly heterogeneous porous media still pose considerable challenges for any numerical method.

[5] Several studies have specifically addressed flow and transport in highly heterogeneous porous media, typically using a "benchmark" configuration and structure: A two- or three-dimensional regular (rectangular) domain with a multi-Gaussian *lnK* and an exponential correlation structure. *Cvetkovic et al.* [1996] analyzed Lagrangian velocity statistics and its deviations from Eulerian velocity statistics in presence of the high heterogeneity with *lnK* variance up to 4, using a hybrid finite element numerical scheme. *Salandin and Fiorotto* [1998] used classic finite element formulation with velocity postprocessor [*Cordes and Kinzelbach*, 1992] and studied flow and advective transport with *lnK* variance up to 4 in order to show Lagrangian and Eulerian velocity statistics and dispersion coefficients. More recently, *de Dreuzy et al.* [2007] extended their work to high-performance 2-D parallel simulations in a large domain and *lnK* variance up to 9, investigating asymptotic behavior of the macrodispersion tensor. A unique methodology was proposed by *Janković et al.* [2003, 2006] and *Fiori et al.* [2006] using a multiindicator structure in three dimensions and addressing effects of high heterogeneity in non-Gaussian *lnK* fields. Moreover, *Zinn and Harvey* [2003] compared flow, dispersion, and mass transfer characteristics in the classic multi-Gaussian field and two non-Gaussian fields with connected either high- and low-conductivity zones, respectively; all having *lnK* variances from 1 to 9. *Trefry et al.* [2003] studied preasymptotic transport behavior for a multi-Gaussian heterogeneity field with $\sigma_Y^2 \leq 4$ and Gaussian correlation structure. Valuable insight was gained from these studies on flow statistics and macroscopic dispersion, in particular that the first-order solutions provide robust estimates for a multi-Gaussian heterogeneity field with *lnK* variance up to 1 [*Wen and Gomez-Hernandez*, 1998].

[6] In this paper we shall take advantage of the new simulation methodology referred to as the adaptive Fup Monte Carlo method (AFMCM) presented by *Gotovac et al.* [2009] and study flow and travel time ensemble statistics in highly heterogeneous porous media with *lnK* variance up to 8; this approach relies on the general adaptive Fup multiresolution framework [*Gotovac et al.*, 2003, 2007, 2009]. Probability density functions (pdf's) of Lagrangian velocity, transverse displacement, and travel time are to be investigated for increasing *lnK* variability. Furthermore, statistical moments for key transport variables are to be analyzed and compared with available first- and second-order results, whereas the simulated probability density functions for key transport variables will be compared with standard distributions, including the solution to the advection-dispersion equation. Particularly, this paper will show that correlation structures of two Lagrangian variables, inverse Lagrangian velocity or slowness and slope, define preasymptotic behavior of the longitudinal and transverse dispersion. Finally, we provide simple estimators for Eulerian and Lagrangian velocity variance, travel time variance, slowness, and longitudinal macrodispersivity applicable for *lnK* variance as high as 8.

2. Problem Formulation

[7] In this paper we shall take advantage of the simulation methodology AFMCM and its high accuracy presented by *Gotovac et al.* [2009] to study experimentally flow and advective transport in a highly heterogeneous porous medium. All relevant flow and transport variables are considered as random space functions (RSFs).

[8] In real aquifers, the heterogeneous structures can typically be very complex, possibly exhibiting high variability, anisotropy, trends, connectivity of extremely low and/or high permeability zones, and three-dimensional non-Gaussian features [e.g., *Gomez-Hernandez and Wen*, 1998]. In this study, we consider a "classical" structure of the hydraulic conductivity, as a reference case for comparison with analytical and other numerical solutions: multi-Gaussian with an exponential covariance, completely defined by first two spatial moments.

[9] The exponential covariance, typically assumed in analytical first- and second-order studies of groundwater flow due to suitable integration properties, abruptly decreases values close to the origin in comparison with other common covariances (e.g., Gaussian as given by *Trefry et al.* [2003]). These effects cause log conductivity fields in each realization to exhibit large spatial contrasts and gradients, which make flow and transport simulations very demanding for any numerical procedure; hence this configuration provides a challenging benchmark for our numerical solution.

[10] Our further simplification is to consider a two-dimensional steady state and "uniform-in-the-average" flow field with a basic configuration illustrated in Figure 1, imposing the following flow boundary conditions: Left and right boundaries are prescribed a constant head, while the top and bottom are no-flow boundaries. The groundwater velocity field $\mathbf{u} = (v_x, v_y)$ is also a RSF with the mean $\mathbf{u}_A$ ($v_{xA} \equiv u$, $v_{yA} \equiv 0$), where the subscript A denotes the arithmetic mean, i.e., $\mathbf{u}_A \equiv \mathrm{E}(\mathbf{u})$ and $u \equiv \mathrm{E}(u)$. This configuration is linked with multi-Gussian *lnK* field and has been extensively studied in the literature [e.g., *Bellin et al.*, 1992; *Salandin and Fiorotto*, 1998; *Hassan et al.*, 1998; *Janković et al.*, 2003; *de Dreuzy et al.*, 2007].

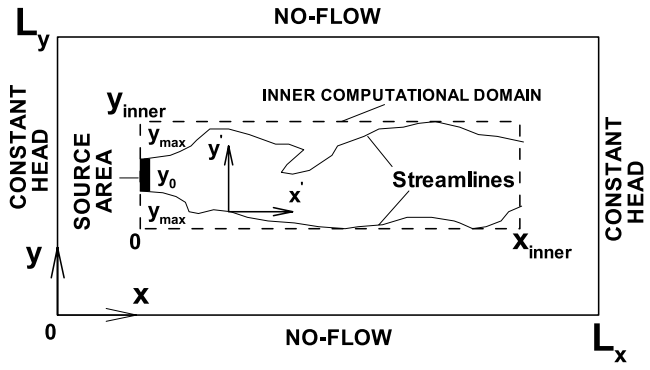

Figure 1. Simulation domain needed for global flow analysis and inner computational domain needed for flow and transport ensemble statistics.

[11] Furthermore, we shall focus on quantifying advective transport using travel time and transverse displacement statistics as functions of the longitudinal distance (i.e., "control plane," parallel to the mean flow) [*Dagan et al.*, 1992; *Cvetkovic et al.*, 1992; *Andricevic and Cvetkovic*, 1998] required frequently in applications such as risk assessment and regulatory analysis. Transport simulations will be performed in the inner computational domain in order to avoid nonstationary influence of the flow boundary conditions (Figure 1). Injection tracer mass is divided to the certain number of particles which all carry the equal fraction of total mass. Particles are injected along the source line and followed downstream such that travel time and transverse displacement are monitored at arbitrary control planes denoted by x.

[12] There are two different injection modes: uniform resident and uniform in-flux [*Kreft and Zuber*, 1978; *Demmy et al.*, 1999]. For brevity, we use terms "resident" and "in-flux" injection mode. For both modes, uniform refers to the homogeneous mass density in the source. "Resident" refers to the volume of resident fluid into which the solute is introduced, while "in-flux" refers to the influent water that carries the solute into the flow domain. Particles are separated by equal distance within the source line for resident and by distance inversely proportional to the specified flow rate between them for in-flux mode [*Demmy et al.*, 1999]. In this study, inert tracer particles are injected instantaneously according to the in-flux injection mode which yields statistically stationary Lagrangian velocities in the entire transport domain; this is in contrast to the resident injection mode where Lagrangian velocity statistics are nonstationary over a significant distance following the source line [*Cvetkovic et al.*, 1996].

[13] In this first application of the AFMCM for analyzing flow and advective transport in heterogeneous porous media, our main interest is (1) to demonstrate the applicability of the method for a "benchmark" configuration and conditions that are familiar in the literature and hence can be compared, both with theoretical and simulation results, and (2) to elucidate some possible new features of advective transport in this simple configuration when *lnK* variance of hydraulic conductivity exceeds 4. The main output stochastic variables are Lagrangian and Eulerian velocity, travel time, and transverse displacement, but also slowness (inverse Lagrangian velocity) and streamline Lagrangian slope which are important for analyzing longitudinal and transversal dispersivity, respectively.

3. Theory

[14] Let $K(\mathbf{x}) = K_G e^{Y(\mathbf{x})}$ define a random space function (RSF) for the hydraulic conductivity where the subscript G denotes the geometric mean and Y is a multi-Gaussian log conductivity field completely represented by two first moments: $N(0, \sigma_Y^2)$ with $C_Y(\mathbf{x}, \mathbf{x}') = \sigma_Y^2 \exp(-|\mathbf{x} - \mathbf{x}'|/I_Y)$. For a given Y, it is a possible to calculate Eulerian velocity statistics for "uniform-in-the-average-flow" defined by pdf or alternatively by mean $\mathbf{u}_A$ ($v_{xA} \equiv u$, $v_{yA} \equiv 0$) and covariances C_{v_x} and C_{v_y}, which are available in closed form as functions of u, σ_Y^2, and I_Y for lower heterogeneity [e.g., *Cvetkovic and Shapiro*, 1990; *Rubin*, 1990]. A consistent first-order approximation yields for the mean velocity $u_A = u = K_G J/n_e$, (where J is a mean hydraulic gradient, n_e is a constant effective porosity, and $u_G \approx u_H \approx u_A$) and for the variances

$$\frac{\sigma_{v_x}^2}{u^2} = \frac{3}{8}\sigma_Y^2$$

$$\frac{\sigma_{v_y}^2}{u^2} = \frac{1}{8}\sigma_Y^2$$

[*Dagan*, 1989]. A complete first-order covariance is given by *Rubin* [1990]. A more complicated second order flow analysis yields

$$\frac{\sigma_{v_x}^2}{u^2} = \frac{3}{8}\sigma_Y^2 + 0.0282\,\sigma_Y^4,$$

$$\frac{\sigma_{v_y}^2}{u^2} = \frac{1}{8}\sigma_Y^2 + 0.041\,\sigma_Y^4,$$

and closed form covariance expressions given by *Hsu et al.* [1996].

[15] Let a dynamically inert and indivisible tracer parcel (or particle) be injected into the transport (inner computational) domain at the source line (say at origin $\mathbf{x} = 0$) for a given velocity field. The tracer advection trajectory can be described using the Lagrangian position vector as a function of time $\mathbf{X}(t) = [X_1(t), X_2(t)]$ [e.g., *Dagan*, 1984] or, alternatively, using the travel (residence) time from $x = 0$ to some control plane at x, $\tau(x)$, and transverse displacement at x, $\eta(x)$ [*Dagan et al.*, 1992]. The τ and η are Lagrangian (random) quantities describing advective transport along a streamline. The advective tracer flux [M/TL] is proportional to the joint probability density function (pdf) $f_{\tau\eta}(\tau, \eta; x)$ [*Dagan et al.*, 1992]. Marginal pdf's $f_\tau = \int f_{\tau\eta}\, d\eta$ and $f_\eta = \int f_{\tau\eta}\, d\tau$ separately quantify advective transport in the longitudinal and transverse directions, respectively. Formally, τ and η are related to X_1 and X_2 as $\tau(x) = X_1^{-1}(x)$ and $\eta(x) = X_2[\tau(x)]$; this description is unique if the tracer particle moves in the direction of the mean flow only, i.e.,

if $X_1(t)$ is a monotonously increasing function implying no backward flow

$$\tau(x;a)=\int_0^x \frac{1}{v_x(\theta,\eta(\theta;a))}d\,\theta;\ \eta(x;a)=\int_0^x \frac{v_y(\theta,\eta(\theta;a))}{v_x(\theta,\eta(\theta;a))}d\,\theta, \tag{1}$$

where $y = a$ is the initial point of a streamline at $x = 0$. This concept is valid from low to mild heterogeneity where $v_x > 0$ [e.g., *Dagan et al.*, 1992; *Guadagnini et al.*, 2003; *Sanchez-Villa and Guadagnini*, 2005].

[16] In the present study, we shall require a more general definition than (1) where τ and η are calculated along streamlines using the total velocity instead of its longitudinal component in order to account for backward flow and multiple crossings. Let l denote the intrinsic coordinate (length) along a streamline/trajectory originating at $y = a$ and $x = 0$; we shall omit a in the following expressions for simplicity. The trajectory function can be parameterized using l as $[X_x(l), X_y(l)]$ and we can write

$$\tau(x)=\int_0^{l(x)} \frac{1}{v\left[X_x(\xi),X_y(\xi)\right]}d\,\xi;\ \eta(x)=\int_0^{l(x)} \frac{v_y\left[X_x(\xi),X_y(\xi)\right]}{v\left[X_x(\xi),X_y(\xi)\right]}d\,\xi. \tag{2}$$

Our focus in the computations will be on the first-passage time; then we can introduce a simple scaling $\xi = (l(x)/x)\,\varsigma \equiv \lambda(x)\,\varsigma$ whereby

$$\tau(x)=\int_0^x \frac{\lambda(x)}{v\left[X_x(\varsigma),X_y(\varsigma)\right]}d\,\varsigma \equiv \int_0^x \alpha(\varsigma;x)\,d\varsigma \tag{3}$$

$$\eta(x)=\int_0^x \frac{v_y\left[X_x(\varsigma),X_y(\varsigma)\right]}{v\left[X_x(\varsigma),X_y(\varsigma)\right]}\lambda(x)\,d\,\varsigma \equiv \int_0^x \beta(\zeta,x)\,d\,\zeta. \tag{4}$$

[17] In (3), α is referred to as the "slowness" or the inverse Lagrangian velocity [T/L], while β in (4) is referred to as the dimensionless streamline slope function, or briefly "slope." It may be noted that in this approach, all Lagrangian quantities depend on space rather than time as in the traditional Lagrangian approach [e.g., *Taylor*, 1921; *Dagan*, 1984]. Scaled velocities defined by $w(\varsigma) \equiv v/\lambda$ and $w_y(\varsigma) \equiv v_y/\lambda$ will be useful for subsequent statistical analysis (in the rest of the paper, we shall refer to $w(\varsigma)$ as "Langrangian velocity"). Note that $l(x)$ is unique as the trajectory length for the first crossing at x.

[18] The first two moments of τ (3) and η (4) are computed as

$$\begin{aligned}\tau_A(x)\equiv E(\tau)&=\int_0^x \alpha_A(\zeta)d\zeta;\ \sigma_\tau^2(x)\equiv E\left[(\tau-\tau_A)^2\right]\\&=\int_0^x\int_0^x C_\alpha(\zeta',\zeta'')d\zeta'd\zeta''\\ \eta_A(x)\equiv E(\eta)=0;\quad \sigma_\eta^2(x)&\equiv E(\eta^2)=\int_0^x\int_0^x C_\beta(\zeta',\zeta'')d\zeta'd\zeta'',\end{aligned} \tag{5}$$

where the covariance functions are defined by

$$C_m(x',x'')\equiv E[m(x')m(x'')]-E[m(x')]E[m(x'')];\ \ (m=\alpha,\beta). \tag{6}$$

The moments of the travel time and transverse displacement are completely defined by the statistics of the slowness and slope; implicit in (5) and (6) is the assumption of statistical stationarity, i.e., integral functions in (5) and (6) are assumed independent of a and x.

[19] The first-order approximation of advective transport is based on the assumption that the streamlines are essentially parallel, i.e., $\eta(x) \approx 0$ and $\lambda \approx 1$, whereby $w \approx v_x(x, 0)$ and $v_y[x, \eta(x)] \approx v_y(x, 0)$, which implies the equivalence of the Eulerian and Lagrangian velocity, with absence of backward flow. Under such conditions, the covariances C_m ($m = \alpha, \beta$) in (5) can be computed as

$$C_\alpha(x',x'')\approx\frac{1}{u^2}C_{v_x}[(x'-x'',0)];\ C_\beta(x',x'')\approx\frac{1}{u^2}C_{v_y}[(x'-x'',0)], \tag{7}$$

where C_{v_x} and C_{v_y} are covariance functions of the Eulerian velocity components v_x and v_y [*Rubin*, 1990], respectively; in (7) we have used the fact that the cross covariance between v_x and v_y is zero [*Rubin*, 1990]. Since at first order $\alpha_A \approx (1/u)_A \approx 1/u$, the first moment of travel time is obtained from (5) as

$$\tau_A(x)=x\alpha_A=x/u=xn_e/K_GJ. \tag{8}$$

[20] Using (5) and (7), the travel time variance is derived in an analogous form as the longitudinal position variance [e.g., *Dagan*, 1989],

$$\frac{\sigma_\tau^2u_A^2}{I_Y^2\sigma_Y^2}=2\chi-3\ln\chi+\frac{3}{2}-3E+3\left[Ei(-\chi)+\frac{(1+\chi)e^{-\chi}-1}{\chi^2}\right], \tag{9}$$

where $\chi \equiv x/I_Y$, $E = 0.5772156649$ is the Euler number, and Ei is the exponential integral. Asymptotic values of σ_τ^2 were derived by *Shapiro and Cvetkovic* [1988].

[21] The first-order result for the transverse displacement variance σ_η^2 is obtained from (5) and (7) in an analogous form as the transverse variance obtained from Lagrangian position analysis [e.g., *Dagan*, 1989]:

$$\frac{\sigma_\eta^2}{I_Y^2\sigma_Y^2}=\ln\chi-\frac{3}{2}+E-Ei(-\chi)+3\left[\frac{1-(1+\chi)e^{-\chi}}{\chi^2}\right]. \tag{10}$$

[22] Finally, we note the empirical relationships for the geometric mean of the Lagrangian velocity [*Cvetkovic et al.*, 1996],

$$\frac{w_g}{u}=1+\frac{\sigma_Y^2}{6}, \tag{11}$$

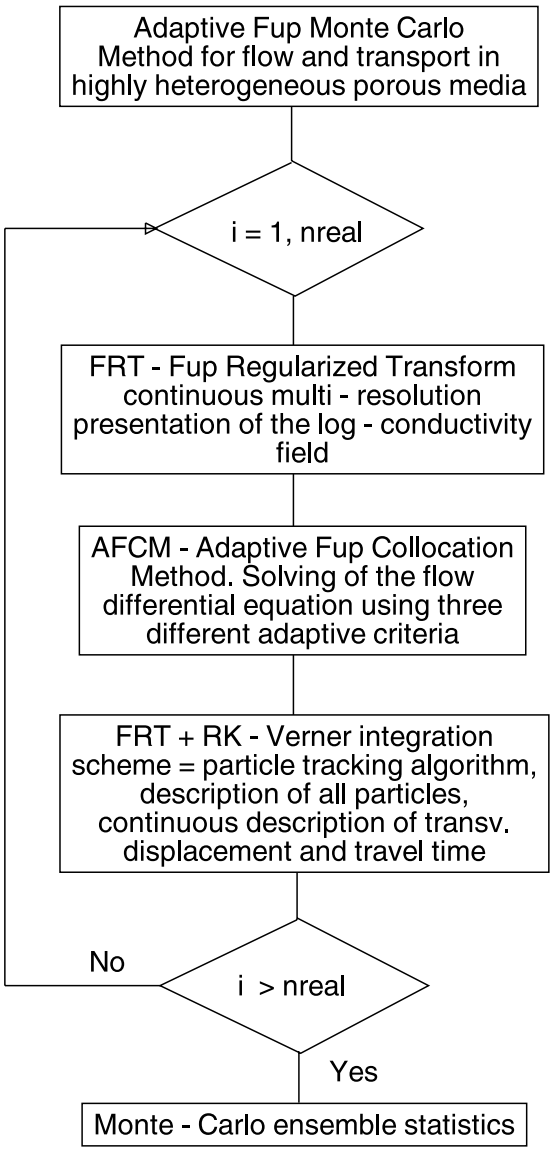

Figure 2. Flowchart of the presented methodology: the adaptive Fup Monte Carlo method (AFMCM).

and variance of the $ln(w)$,

$$\sigma^2_{\ln(w)} = 2\ln\left(1+\frac{\sigma^2_Y}{6}\right). \quad (12)$$

4. Computational Framework

4.1. Monte Carlo Methodology

[23] Our new simulation methodology, referred to as the adaptive Fup Monte Carlo method (AFMCM) and presented by *Gotovac et al.* [2009], supports the Eulerian-Lagrangian formulation which separates the flow from the transport problem and consists of the following common steps [*Rubin*, 2003]: (1) generation of as high number as possible of log conductivity realizations with predefined correlation structure, (2) numerical approximation of the log conductivity field, (3) numerical solution of the flow equation with prescribed boundary conditions in order to produce head and velocity approximations, (4) evaluation of the displacement position and travel time for a large number of the particles, (5) repetition of steps 2–4 for all realizations, and (6) statistical evaluation of flow and transport variables such as head, velocity, travel time, transverse displacement, solute flux, or concentration (including their cross moments and pdf's).

[24] Figure 2 shows the flowchart of the AFMCM, which represents a general framework for flow and transport in heterogeneous porous media. The methodology is based on Fup basis functions with compact support (related to the other localized basis functions such as splines or wavelets) and Fup collocation transform (FCT), which is closely related to the discrete Fourier transform and can simply represent, in a multiresolution way, any signal, function, or set of data using only few Fup basis functions and resolution levels on nearly optimal adaptive collocation grid resolving all spatial and/or temporal scales and frequencies. Fup basis functions and FCT were presented in detail by *Gotovac et al.* [2007]. New or improved Monte Carlo methodology aspects are (1) Fup regularized transform (FRT) for data or function (e.g., log conductivity) approximation in the same multiresolution way as FCT, but computationally more efficient, (2) novel form of the adaptive Fup collocation method (AFCM) for approximation of the flow differential equation, (3) new particle tracking algorithm based on Runge-Kutta-Verner explicit time integration scheme and FRT, and (4) Monte Carlo (MC) statistics represented by Fup basis functions. All mentioned MC methodology parts are presented by *Gotovac et al.* [2009].

[25] Finally, AFMCM uses a random field generator HYDRO_GEN [*Bellin and Rubin*, 1996] for step 1, FCT or FRT for log conductivity approximation (step 2), AFCM for the differential flow equation (step 3), new particle tracking algorithm for transport approximations for step 4, and statistical properties of the Fup basis functions for step 6 (Figure 2).

4.2. Experimental Setup

[26] Figure 1 shows flow and inner transport domain, while Table 1 presents all input data needed for Monte Carlo simulations. Experimental setup presented here is based on convergence and accuracy analysis of Appendix A and *Gotovac et al.* [2009].

[27] Figure 1 shows a 2-D computational domain for steady state and unidirectional flow simulations using three sets of simulations defined on domains $64I_Y \times 32I_Y$, $128I_Y \times 64I_Y$, and $64I_Y \times 128I_Y$ (I_Y is the integral scale; Table 1), imposing the following boundary conditions: Left and right boundaries are prescribed a constant head, while the top and bottom are no-flow boundaries. The random field generator HYDRO_GEN [*Bellin and Rubin*, 1996] generates *lnK* fields for six discrete values of *lnK* variance: 0.25, 1, 2, 4, 6, and 8; for simplicity, the porosity will be assumed uniform. *Gotovac et al.* [2009] defines discretization or resolution for *lnK* and head field for domain $64I_Y \times 32I_Y$ in order to get accurate velocity solutions for particle tracking algorithm (Table 1); $n_Y/I_Y = 4$ (four collocation points per integral scale) and $n_h/I_Y = 16$ for low and mild heterogeneity ($\sigma^2_Y \leq 2$) and $n_Y/I_Y = 8$ and $n_h/I_Y = 32$ for high heterogeneity ($\sigma^2_Y > 2$). For other two set of simulations on

Table 1. All Input Data for Monte Carlo Simulations

Flow Domain	First Set (Simulations 1–6), $64I_Y \times 32I_Y$						Second Set (Simulations 7–9), $128I_Y \times 64I_Y$			Third Set (Simulation 10), $64I_Y \times 128I_Y$
	1, $\sigma_Y^2 = 0.25$	2, $\sigma_Y^2 = 1$	3, $\sigma_Y^2 = 2$	4, $\sigma_Y^2 = 4$	5, $\sigma_Y^2 = 6$	6, $\sigma_Y^2 = 8$	7, $\sigma_Y^2 = 4$	8, $\sigma_Y^2 = 6$	9, $\sigma_Y^2 = 8$	10, $\sigma_Y^2 = 8$
n_Y/I_Y	4	4	8	8	8	8	4	4	4	4
n_h/I_Y	16	16	16	32	32	32	16	16	16	16
Inner domain	$40I_Y \times 26I_Y$	$40I_Y \times 26I_Y$	$40I_Y \times 24I_Y$	$40I_Y \times 20I_Y$	$40I_Y \times 18I_Y$	$40I_Y \times 16I_Y$	$100I_Y \times 52I_Y$	$100I_Y \times 46I_Y$	$100I_Y \times 40I_Y$	$40I_Y \times 96I_Y$
N_p	1000	1000	1000	4000	4000	4000	4000	4000	4000	4000

larger domains we use $n_Y/I_Y = 4$ and $n_h/I_Y = 16$ for high heterogeneity in order to keep 2.1×10^6 head unknowns in each realization, which is our current computational limit (Table 1), but still maintaining a relatively accurate velocity solution according to *Gotovac et al.* [2009].

[28] Transport simulations will be performed in the inner domain in order to avoid nonstationary influence of the flow boundary conditions. Appendix A shows particular analysis which finds an inner computational domain for all three sets of simulations implying flow criterion that each point of the inner domain must have constant Eulerian velocity variance (Table 1, Figure A1). Figure A2 shows that for high heterogeneity all domains ensure similar travel time results, while larger transversal dimensions are needed for reliable transverse displacement statistics. All simulations use up to $N_P = 4000$ particles, $n_{MC} = 500$ Monte Carlo realizations and relative accuracy of 0.1% for calculating τ and η in each realization in order to minimize statistical fluctuations [*Gotovac et al.*, 2009, Table 1]. Source area (or line; $y_0 = 12I_Y$) is located in the middle of the left side of the inner domain and is sufficiently small that injected particles do not fluctuate outside the inner domain and sufficiently large such that change in transport ensemble statistics due to source size is minimized (Table 1, Figure A3). Finally, as mentioned above, in-flux injection mode is used, which imply that position of each particle (y_i) in the local coordinate system of source line can be obtained solving the following nonlinear equation:

$$i = N_P \int_0^{y_i} v_x(0,y)\, dy \Big/ \int_0^{y_0} v_x(0,y)\, dy \quad (i = 0, \ldots, N_P)$$

[*Demmy et al.*, 1999].

[29] The cumulative distribution function (CDF) of the travel time is to be computed as

$$F_\tau(t;x) = E(H(t-\tau(x)) = \frac{1}{N_P n_{MC}} \sum_{i=0}^{N_P} \sum_{j=1}^{n_{MC}} (H(t-\tau(x))), \quad (13)$$

where H is a Heaviside function, N_P is number of particles, n_{MC} is number of Monte Carlo realizations, while travel time in (13) has the form (3) for each particular particle and realization; therefore expectation in (13) is made over all realizations and particles from the source. Probability density function (pdf) is simply obtained as $f_\tau(t;x) = \partial(F_\tau(t;x))/\partial t$. Analogous procedure is applied for all other Lagrangian variables such as transverse displacement, Lagrangian velocity, slowness and slope. Because of stationarity, Eulerian velocity pdf is calculated over the whole inner computational domain and all realizations are as in Appendix A. Detailed description of Monte Carlo statistics using AFMCM is presented by *Gotovac et al.* [2009].

5. Transport Statistics

5.1. Travel Time

[30] Appendix A shows that all three sets of simulations give practically the same travel time statistics. Therefore here we show high-resolution travel time results for domain $64I_Y \times 32I_Y$ and other related input data in Table 1 (simulations 1–6).

[31] Dimensionless mean travel time is closely reproduced with expression (8) for all considered σ_Y^2. The dimensionless travel time variance as a function of distance is illustrated in Figure 3 where a comparison is made with the first-order solution (9). The simulated variance is a nonlinear function of the distance from the source only, say, up to about $5I_Y$, after which it attains a near-linear dependence. Interestingly, the nonlinear features of σ_τ^2 with distance diminish as σ_Y^2 increases: The discrepancy of the simulated σ_τ^2 from a line set at the origin is larger for, say, $\sigma_Y^2 = 2$ (Figure 3a) than for $\sigma_Y^2 = 8$ (Figure 3b); this σ_τ^2 behavior will be explained in the sequel with respect to the slowness correlation (equation (5)).

[32] The comparison with the first-order solutions indicates, consistent with earlier studies, that up to $\sigma_Y^2 = 1$, equation (9) reproduces simulated values reasonably well, although some deviations are visible even for $\sigma_Y^2 = 0.25$ (Figure 3a). With increasing σ_Y^2, the deviations are significantly larger between the simulated and first-order solution (relative error $\varepsilon_r = (\sigma^2_{\tau,AFMCM} - \sigma^2_{\tau,1})/\sigma^2_{\tau,AFMCM}$ of the first-order theory is only 4.7% for $\sigma_Y^2 = 0.25$, 13.3% for $\sigma_Y^2 = 1$, but even 65.6% for $\sigma_Y^2 = 8$; Figure 3b). Actually, the first-order variance is relatively accurate and robust for low heterogeneity up to $\sigma_Y^2 = 1$. Note that σ_τ^2 in Figure 3 retains a concave form, in contrast to the case of particle injection in the resident injection mode, where the variance σ_τ^2 attains a convex form within the first 7–12 integral scales [*Cvetkovic et al.*, 1996]. The main reason for the difference is the nonstationarity of the Lagrangian velocity and slowness for resident injection mode. For in-flux injection, the Lagrangian velocity and slowness are stationary and consequently the travel time variance attains a linear form already after a few integral scales [*Demmy et al.*, 1999]. Impact of the

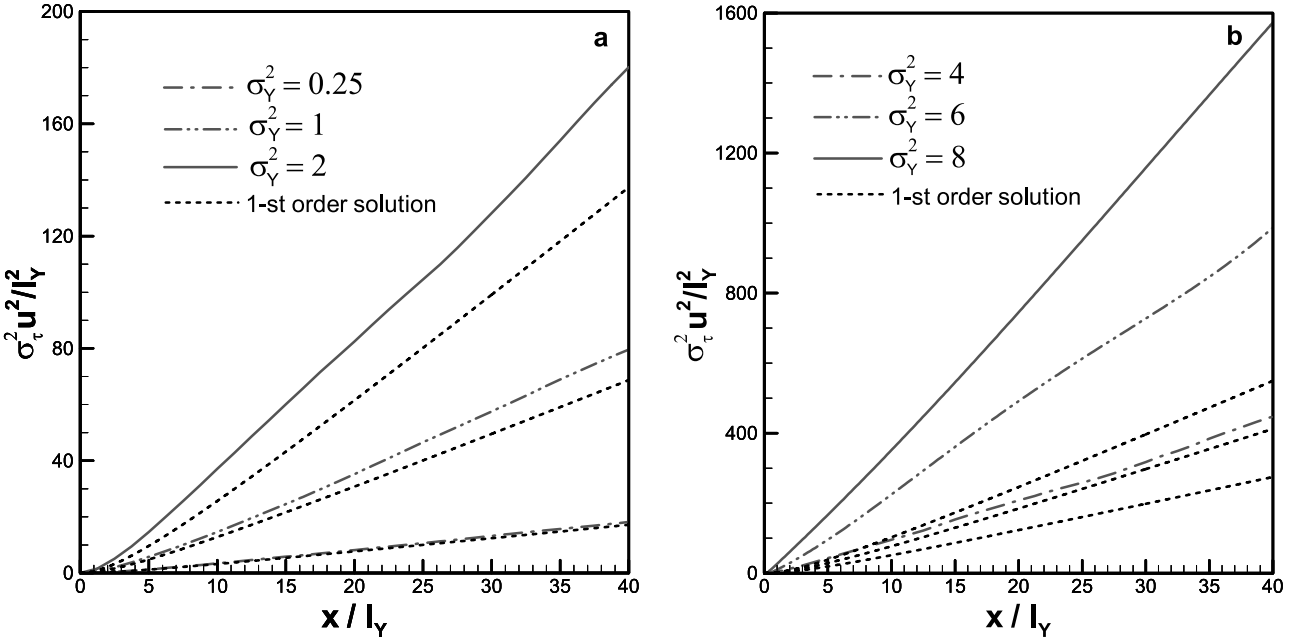

Figure 3. Dimensionless travel time variance (AFMCM and first-order solution): (a) $\sigma_Y^2 = 0.25$, 1, and 2, and (b) $\sigma_Y^2 = 4$, 6, and 8. Simulations 1–6 are used (Table 1).

Lagrangian velocity and slowness will be further discussed in sections 7 and 9.

[33] The travel time probability density functions (pdf's) are illustrated on a log-log plot for three chosen control planes and all considered σ_Y^2 in Figure 4. Deviations from a symmetrical distribution (e.g., lognormal) decrease with distance from the source area, and increase significantly with increasing σ_Y^2. For low heterogeneity (Figures 4a and 4b), small deviations from a symmetric distribution occur only within the first 10–20 integral scales, while almost complete symmetry is attained after 40 integral scales. For mild heterogeneity (Figure 4c) asymmetry of the travel time density become larger, diminishing with increasing distance; at around 40 integral scales a symmetric distribution approximates well the simulated pdf. For high heterogeneity (Figures 4d–4f) the computed pdf is increasingly asymmetric, with both the early and late arrival shifted to later times. Although the asymmetry in the pdf diminishes with increasing distance, for high heterogeneity it is still maintained over the entire considered domain of $40I_Y$. The second set of simulations with larger longitudinal domain of $100I_Y$ does not show significantly smaller deviations between the actual travel time pdf and lognormal approximation.

[34] The travel time density exhibits power law tailing with an increasing (steeper) slope for larger distance. The inferred slopes are summarized in Table 2 for all considered σ_Y^2 and three locations ($x/I_Y = 10$, 20, and 40). All slopes are higher than 3:1, implying that in spite of a power law asymptotic form, advective transport under investigated conditions is not anomalous even for the highest σ_Y^2 considered [*Scher et al.*, 2002; *Fiori et al.*, 2007].

5.2. Transverse Displacement

[35] Appendix A shows that transverse spreading is very sensitive to the transversal size of the domain. Therefore we use the largest required domain for high heterogeneity cases ($\sigma_Y^2 > 2$) as stated in section 4.2 (simulations 1–3, 7–8, and 10; see also Table 1) in order to satisfy flow and transport criteria. The first moment of the transverse displacement η is close to zero with maximum absolute values less than $0.1I_Y$. Figure 5a shows dimensionless transverse displacement variance σ_η^2 for all control planes and considered σ_Y^2. Variance σ_η^2 increases nonlinearly with distance and its form as a function of x is in qualitative agreement with the first-order solution. The magnitude of σ_η^2 is underestimated by the first-order results with relative error of 12.8% for $\sigma_Y^2 = 0.25$ and 39.4% for high heterogeneity.

[36] Figures 5b–5d show transverse displacement pdf ($\sigma_Y^2 = 1$, 4, and 8) at three different control planes ($x/I_Y = 1$, 5, and 40). Generally, the transverse displacement pdf shows a higher peak and wider tailings compared with the normal distribution, mainly due to streamline fluctuations around the mean and flow channeling. These deviations are more significant for very close control planes ($x/I_Y < 10$) and high heterogeneity cases ($\sigma_Y^2 \geq 4$). Moreover, for $x/I_Y > 20$, transverse displacement is found to be very close to the normal distribution, even in a case of high heterogeneity [*Cvetkovic et al.*, 1996]. This behavior is also shown in Table 3 with respect to the kurtosis coefficient and $\sigma_Y^2 = 8$. Kurtosis is relatively high for very close control planes implying sharper peak around the mean, while for $x/I_Y > 20$ kurtosis is close to 3, implying convergence to the normal distribution.

6. Flow Statistics

[37] If integral expressions for travel time and transverse displacement (1) are written in a discrete form, e.g., as

$$\tau(x) = \sum_{i=0}^{N} \alpha_i \Delta x_i,$$

we obtain a form consistent with a random walk representation of transport [e.g., *Scher et al.*, 2002]. Of particular

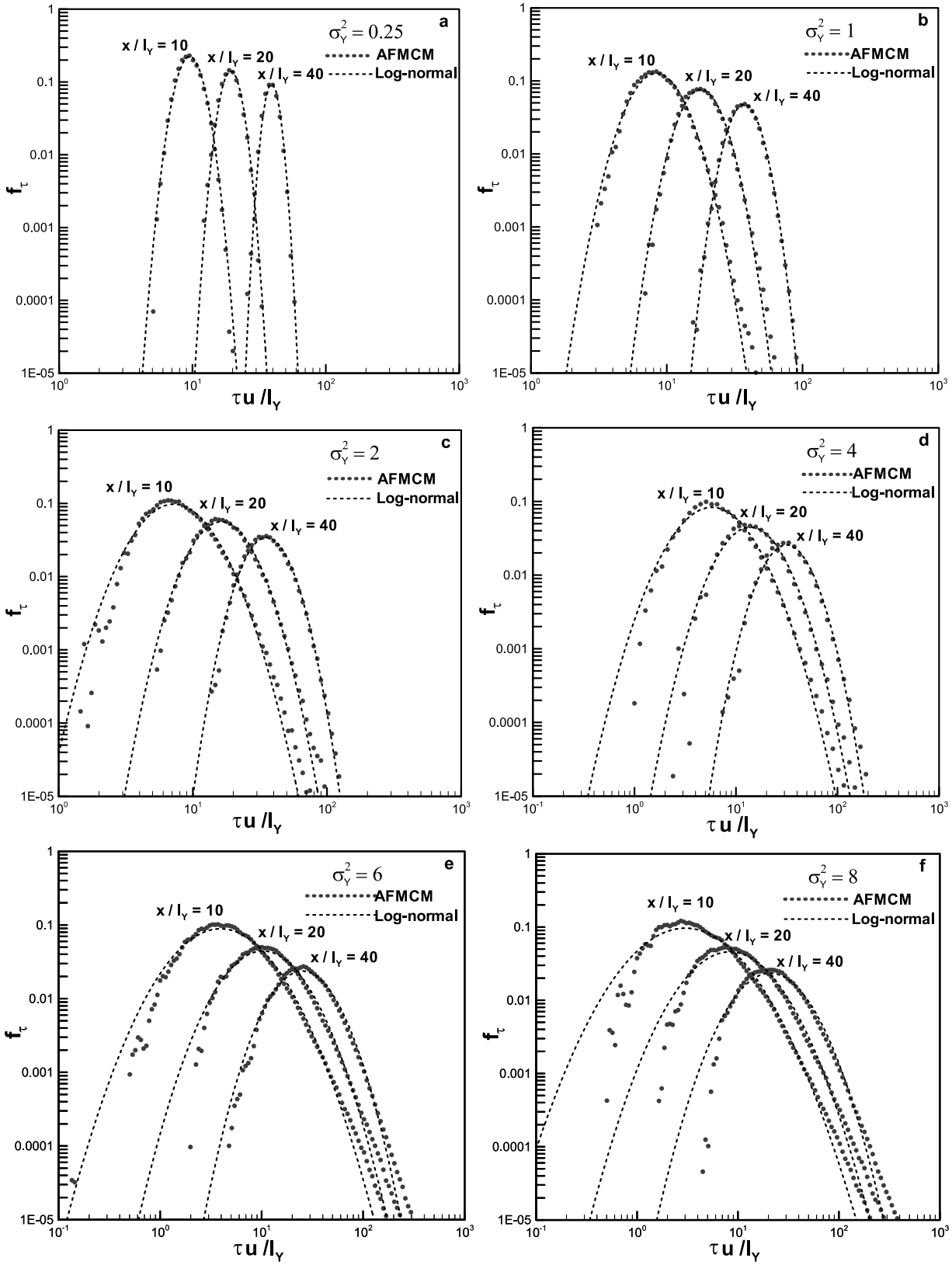

Figure 4. Travel time probability density function (pdf) for three different control planes and all considered σ_Y^2 in log-log scale including comparison with lognormal distribution. Simulations 1–6 are used (Table 1).

Table 2. Travel Time Probability Density Function Asymptotic Slopes for Different *lnK* Variances and Control Planes[a]

σ_Y^2	4	6	8
$x/I_Y = 10$	4.21:1	3.43:1	3.07:1
$x/I_Y = 20$	4.67:1	3.62:1	3.37:1
$x/I_Y = 40$	5.68:1	4.20:1	3.54:1

[a]Simulations 1–6 are used.

Table 3. Kurtosis for Transverse Displacement Probability Density Function and $\sigma_Y^2 = 8$[a]

x/I_Y	Kurtosis (η)
1	9.675
2	5.631
5	4.174
10	3.522
20	3.204
40	3.025

[a]Simulation 10 is used.

significance is that we use a Cartesian coordinate x as the independent variable, and thus the domain can be defined with a specified number of segments of a constant or variable length, and a particle is viewed as performing jumps (''hops'') from one segment to the next. In such a representation of advective transport, the key statistical quantities are α and β. Furthermore, the segment length (constant or variable) needs to be appropriately defined in relation to the integral scales of the Lagrangian velocity field. Without attempting to pursue such analysis at this time, we shall take advantage of the proposed AFMCM approach in order to study the flow statistics, first of the

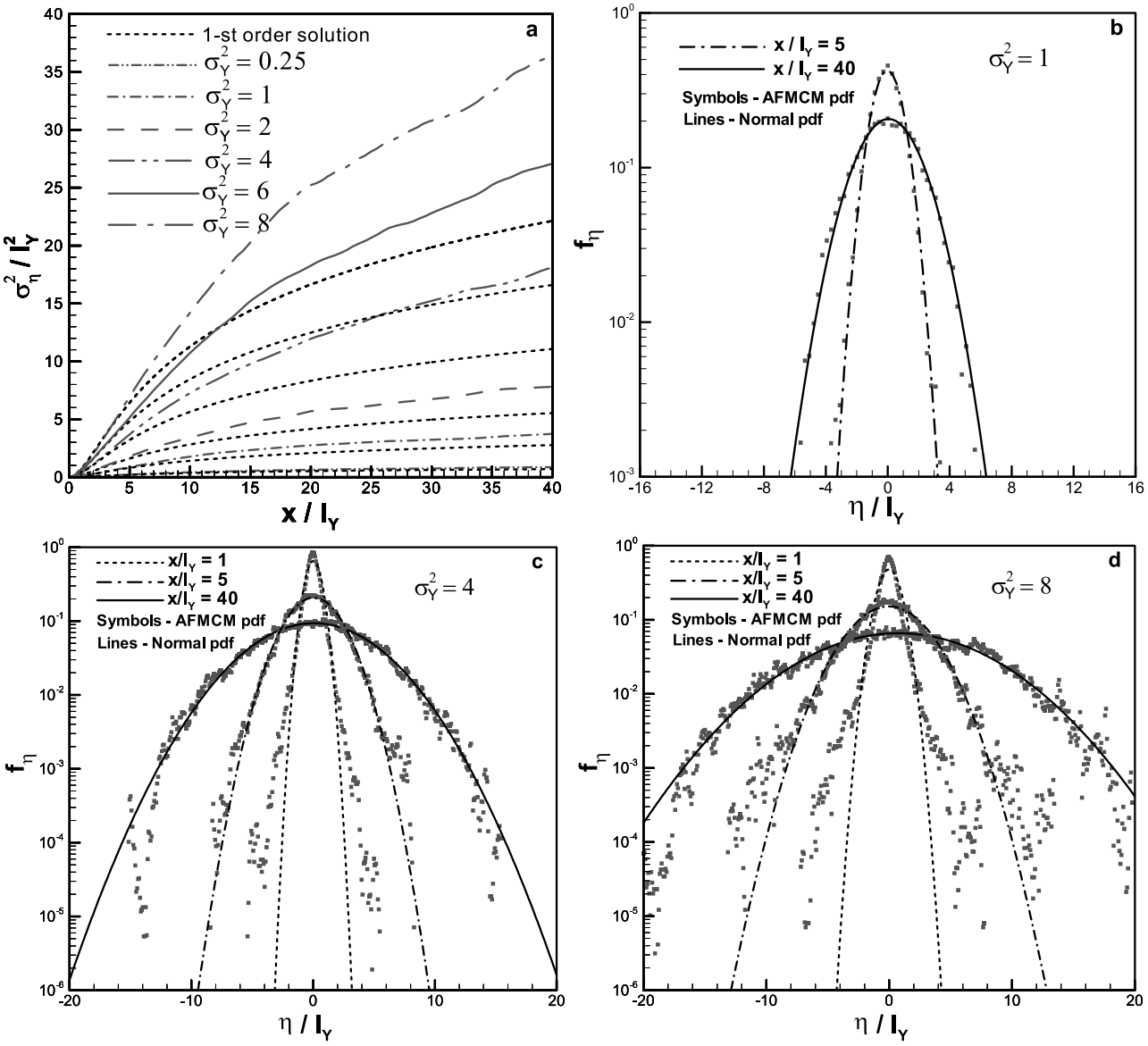

Figure 5. Dimensionless transverse displacement: (a) variance for all considered σ_Y^2, pdf's in semilog scale for different control planes and (b) $\sigma_Y^2 = 1$, (c) $\sigma_Y^2 = 4$, and (d) $\sigma_Y^2 = 8$. Simulations 1–3, 7–8, and 10 are used (Table 1).

velocity field, and then more significantly, of the slowness α with emphasis on travel time and longitudinal dispersion, and slope β with emphasis on transverse displacement and transverse dispersion. Simulations 1–6 are used for all variables; apart from β which use simulations 1–3, 7–8, and 10 (Table 1). It means that both velocities share the same area, i.e., inner computational domain as specified in Figures 1 and A1 where Eulerian velocity is stationary. Eulerian velocity statistics are calculated in collocation points of head solution within the inner domain. On the other side, Lagrangian velocity and other Lagrangian variables are calculated using the certain number of particles and control planes as specified in Table 1. Because of the weak stationarity of log conductivity field that correlation depends only on the separation between two points, rather than its actual positions, both velocities share the same property. Consequently, mean, variance, and pdf are stationary for all points for Eulerian velocity or control planes for Lagrangian velocity in the inner domain which significantly simplifies this analysis.

6.1. Mean and Variance

[38] Figure 6a illustrates how different dimensionless mean velocities change with increasing σ_Y^2. Arithmetic mean of v_x/u and v_y/u is unity and zero, respectively [*Dagan*, 1989]. Discrepancy between theoretical and numerical results is the first indicator of numerical error (<3% even for high-heterogeneity cases; see *Gotovac et al.* [2009]). Geometric mean of the dimensionless Lagrangian velocity w/u increases linearly, while Eulerian geometric mean decreases nonlinearly with increasing σ_Y^2, due to the formation of preferential flow "channels." An empirical expression for geometric mean of Lagrangian velocity suggested by *Cvetkovic et al.* [1996, equation (11)] appears as a good estimator, even for $\sigma_Y^2 > 4$. Note that arithmetic mean of αu and β is unity and zero, respectively.

[39] In Figures 6b–6d the dependence of velocity-related variances on σ_Y^2 is illustrated. The Eulerian velocity variance is bounded by the first-order [*Rubin*, 1990] and second-order [*Hsu et al.*, 1996] results as lower and upper limit, respectively (Figures 6b and 6c). The first-order solution is accurate for low heterogeneity cases $\sigma_Y^2 < 1$ and acceptable for mild heterogeneity with $\sigma_Y^2 \leq 2$ (relative error less than 10% for longitudinal velocity, but up to 34% for transverse velocity). The second-order solution is accurate and robust for low and mild heterogeneity, but not appropriate for high heterogeneity (for $\sigma_Y^2 = 4$ relative error is around 19% for transversal velocity).

[40] Generally, both analytic solutions better approximate longitudinal than the transverse velocity variance. Numerical results of *Salandin and Fiorotto* [1998] agree quite well with our results up to $\sigma_Y^2 \leq 4$, especially for transverse variance. Their longitudinal variance is slightly higher than the second-order theory, which may be a consequence of the small numerical error. Recent numerical results of *de Dreuzy et al.* [2007] which used $\sigma_Y^2 \leq 9$ are in a close agreement with *Salandin and Fiorotto* [1998] for σ_Y^2 up to 4, but they did not report results for $\sigma_Y^2 > 4$. J. R. de Dreuzy et al. (personal communication, 2008) calculated flow statistics in a single realization of a large domain ($409.6I_Y \times 409.6I_Y$ and $n_Y = 10$). They obtained 6–8% smaller variances than published MC results with 100 realizations [*de Dreuzy et al.*, 2007], explaining this difference as a lack of the extreme velocity values in the single realization. Furthermore, *Zinn and Harvey* [2003] reported smaller variance values than *de Dreuzy et al.* [2007], although they used the same block-centered finite difference procedure. Nevertheless, we can conclude that our velocity variances are in a good agreement with J. R. de Dreuzy et al. (personal communication, 2008) for high heterogeneity in a wide range of $\sigma_Y^2 \in [0, 8]$. We are now in position to provide simple estimator for Eulerian variances in the form suggested by *Hsu* [2004],

$$\frac{\sigma_i^2}{u^2} = \sigma_i^{2\,[1]}\left(1 + \frac{1}{c}\frac{\sigma_i^{2[2]}}{\sigma_i^{2[1]}}\right)^c \quad ; \quad i = v_x, v_y, \tag{14}$$

where the superscript in brackets denotes variance corrections obtained by the first- and second-order presented in section 3, while c is an unknown real number which can be calibrated using MC results. We obtain c as 0.175 and 0.535 for longitudinal and transversal Eulerian variance, respectively, whereby

$$\frac{\sigma_{v_x}^2}{u^2} = \frac{3}{8}\sigma_Y^2\left(1 + \frac{1}{0.175}\frac{0.0282\,\sigma_Y^4}{(3/8)\,\sigma_Y^2}\right)^{0.175} = \frac{3}{8}\sigma_Y^2\left(1 + \frac{376}{875}\sigma_Y^2\right)^{0.175} \tag{15}$$

$$\frac{\sigma_{v_y}^2}{u^2} = \frac{1}{8}\sigma_Y^2\left(1 + \frac{1}{0.535}\frac{0.041\,\sigma_Y^4}{(1/8)\,\sigma_Y^2}\right)^{0.535} = \frac{1}{8}\sigma_Y^2\left(1 + \frac{328}{535}\sigma_Y^2\right)^{0.535}. \tag{16}$$

Figures 6b–6c show that estimators (15) and (16) reproduce reasonably well MC results.

[41] Figure 6b shows dimensionless variance of log-Lagrangian velocity for which empirical expression given by *Cvetkovic et al.* [1996, equation (12)] appears as a good estimator, even for $\sigma_Y^2 > 4$. Figure 6c presents variance of the slope function which is smaller than one and increases as σ_Y^2 increases due to more variable flow in transversal direction. Figure 6d presents dimensionless variances of Lagrangian velocity and slowness which are significantly larger than Eulerian velocity variances. Note that all mean and variances show stationarity with same values in all control planes due to used in-flux injection mode. On the other side, *Cvetkovic et al.* [1996] used resident mode and reported Lagrangian nonstationarity within first $7–12I_Y$. In section 7 we shall take advantage of the relatively simple dependency of $\sigma_\alpha^2 u$ on σ_Y^2 as given in Figure 6d to derive an estimator for longitudinal dispersion.

6.2. Correlation

[42] The correlation of the Eulerian velocity components v_x and v_y is illustrated in Figures 7a and 7b, respectively, for different σ_Y^2. Longitudinal velocity correlation function in the x direction decreases with increasing σ_Y^2 (Figure 7a) due to change in velocity structure by preferential flow. In Figure 7b, high heterogeneity yields a diminishing "hole effect." It is important to note, however, that in contrast to the correlation function, the covariance function increases with σ_Y^2 because variance (Figures 6b and 6c) more rapidly increases than correlation function decreases for large σ_Y^2.

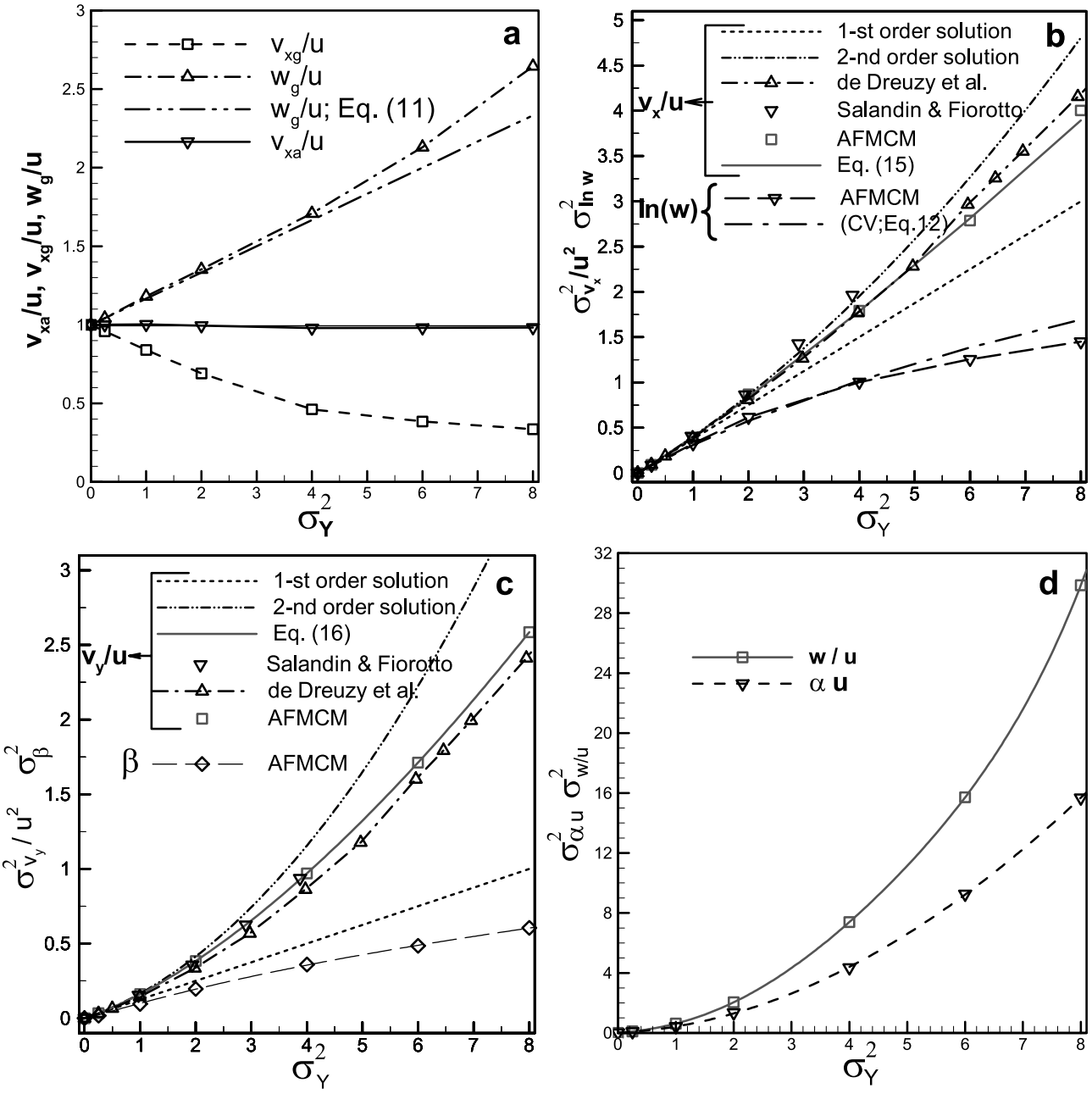

Figure 6. First two Eulerian and Langrangian velocity moments as a function of σ_Y^2: (a) arithmetic and geometric means, variance values of (b) v_x/u and $ln(w)$, (c) v_y/u and β, and (d) αu and w/u. Equations (11)–(12) from *Cvetkovic et al.* [1996] are included in order to estimate geometric mean and variance of the Lagrangian velocity, respectively. Equations (15) and (16) present estimators for the AFMCM Eulerian velocity longitudinal and transversal variance, respectively. Solutions of Eulerian velocity variances of *Salandin and Fiorotto* [1998] and J. R. de Dreuzy et al. (personal communication, 2008) are also included. Simulations 1–6 are used for all variables, apart from β which use simulations 1–3, 7–8, and 10 (Table 1).

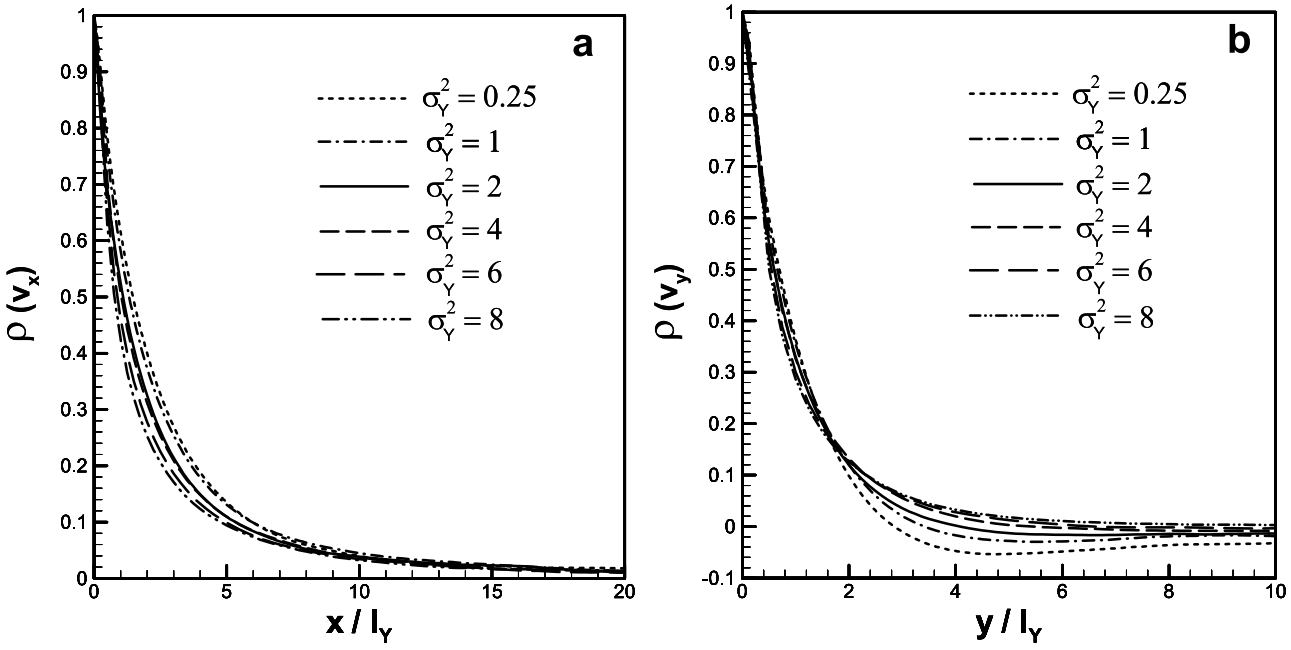

Figure 7. Correlation functions for all considered σ_Y^2: (a) longitudinal Eulerian velocity in the x direction, and (b) transverse Eulerian velocity in the y direction. Simulations 1–6 are used for all variables (Table 1).

Recalling Figure 14 of *Gotovac et al.* [2009], we can conclude that first- and second-order theory provides upper and lower covariance limits, respectively; however, for high heterogeneity these approximations are poor.

[43] Figures 8a–8d illustrate correlation functions of Lagrangian velocity w, slowness α, and slope β, for different σ_Y^2. Lagrangian velocity correlation function increases with increasing σ_Y^2 (Figure 8a), contrary to the Eulerian longitudinal velocity component (Figure 7a). Thus the opposing effect of increasing σ_Y^2 on the correlation function of v_x and w clearly demonstrates the effect of increasingly persistent flow along preferential channels.

[44] Correlation of the slowness α decreases with increasing of σ_Y^2 (Figures 8b and 8c), which has a direct effect on the longitudinal dispersion quantified by the travel time variance (section 7). Furthermore, travel time variance is a completely defined by the covariance of the slowness (equation (5)). Figures 8b and 8c indicate a relatively small slowness correlation length and integral scale, approximately equal to the integral scale of log conductivity. Therefore integration of equation (5) yields only after a few I_Y a near-linear travel time variance. After $30I_Y$, slowness correlation reaches zero for all considered σ_Y^2. The travel time variance asymptotically reaches a linear form after about $60I_Y$. Because of decreasing of the slowness correlation with increasing σ_Y^2, the travel time variance reaches an asymptotic linear shape at a smaller distance for higher σ_Y^2, which is intuitively unexpected and principally enables more efficient calculation of the longitudinal dispersion than in the classical "temporal" Lagrangian approach [see *de Dreuzy et al.*, 2007].

[45] Figure 8d presents slope correlation for high heterogeneity cases $\sigma_Y^2 \geq 4$. The slope correlation shows "hole effect" with integral scale which converges to zero. Correlation does not change significantly with increasing σ_Y^2, approaching zero correlation between 4 and $5I_Y$. By definition of equation (5), transverse displacement variance asymptotically reaches constant sill if integral scale of the slope function converges to zero. Impact of the slope correlation and transverse displacement variance on transverse dispersion will be shown in section 8.

6.3. Distribution

[46] Eulerian and Lagrangian velocity pdf's are illustrated on a log-log plot in Figures 9a and 9b for a low and high σ_Y^2. Negative values of Eulerian longitudinal velocity are discarded because pdf is significantly closer to the lognormal than normal pdf. The two pdf's are very similar for small heterogeneity as assumed by first-order theory [*Dagan*, 1989], but significant differences arise for high heterogeneity ($\sigma_Y^2 > 3$) (Figure 9b). Once again, the divergence of the v_x and w pdf's with increasing σ_Y^2 indicate preferential flow or channeling [*Moreno and Tsang*, 1994; *Cvetkovic et al.*, 1996]: The Lagrangian velocity pdf reflects a higher proportion of larger velocities pertinent to the trajectories. By contrast, Eulerian velocity pdf reflects a significant part of low velocities, since preferential flow channels occupy only a relatively small portion of the domain. A lognormal distribution appears to be a satisfactory model only in the case of the small heterogeneity; deviations are significant for mild and especially high heterogeneity due to enhanced asymmetry of the simulated pdf (Figure 9b). Therefore differences between Eulerian and Lagrangian velocity pdf, as well as pdf deviations from the lognormal distribution, are indicators of preferential flow and channeling.

[47] Slowness (α) pdf shows similar characteristics as the Lagrangian velocity (w) pdf concerning its shape, deviations from the lognormal distribution, and its tailing (Figures 9c and 9d). Slope (β) pdf shows symmetric and nearly normal distribution for low heterogeneity (Figure 9e). High heterogeneity (Figure 9f) causes strongly nonnormal behavior implying a more uniform pdf and different shape of the

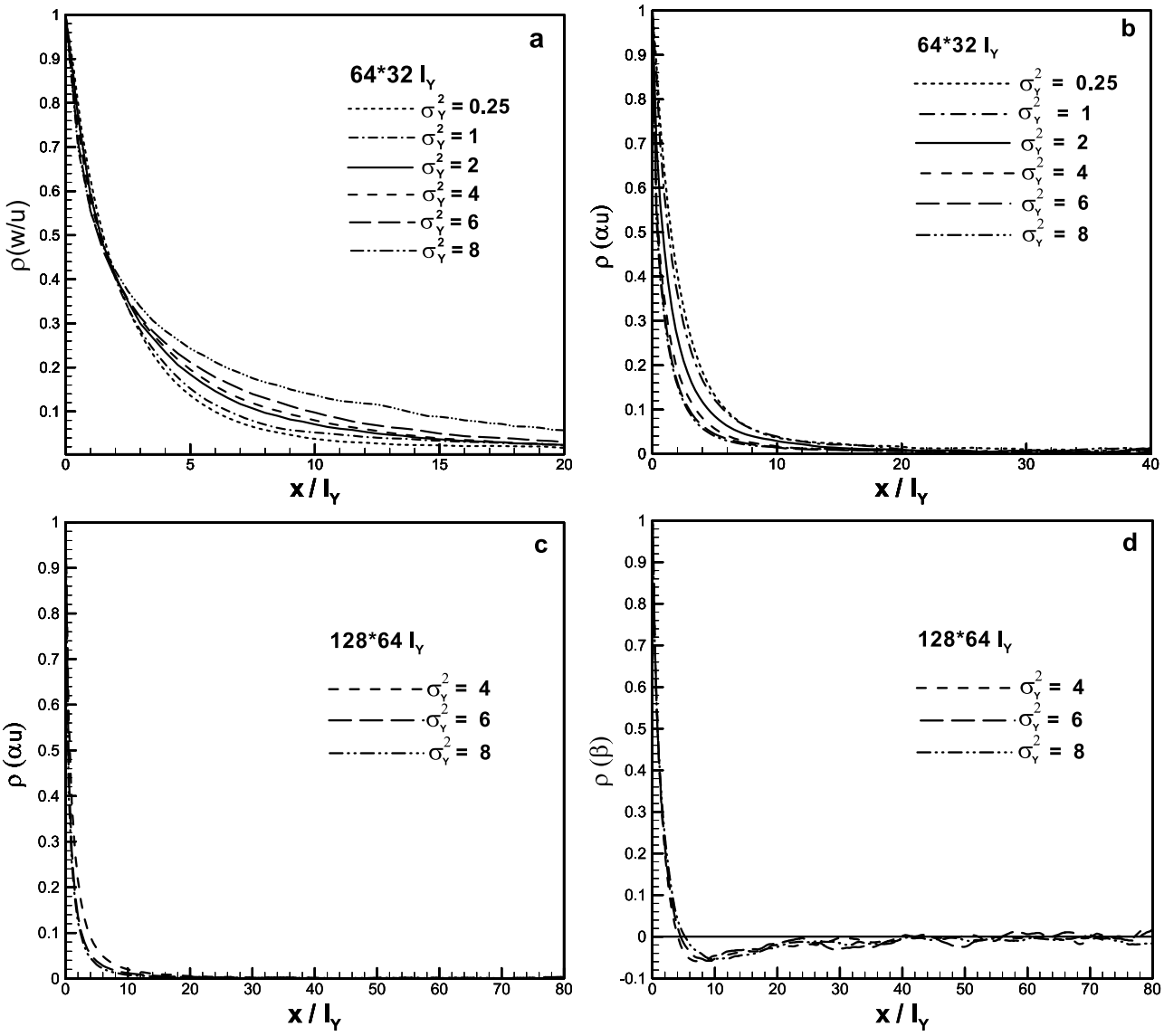

Figure 8. Correlation functions for different σ_Y^2 in the streamline longitudinal direction: (a) Langrangian velocity for domain $64I_Y \times 32I_Y$, (b) slowness or inverse Langrangian velocity for domain $64I_Y \times 32I_Y$, (c) slowness for domain $128I_Y \times 64I_Y$, and (d) slope for domain $128I_Y \times 64I_Y$. Simulations 1–6 are used for all variables for Figures 8a and 8b. Simulations 7–8 and 10 are used for all variables for Figures 8c and 8d.

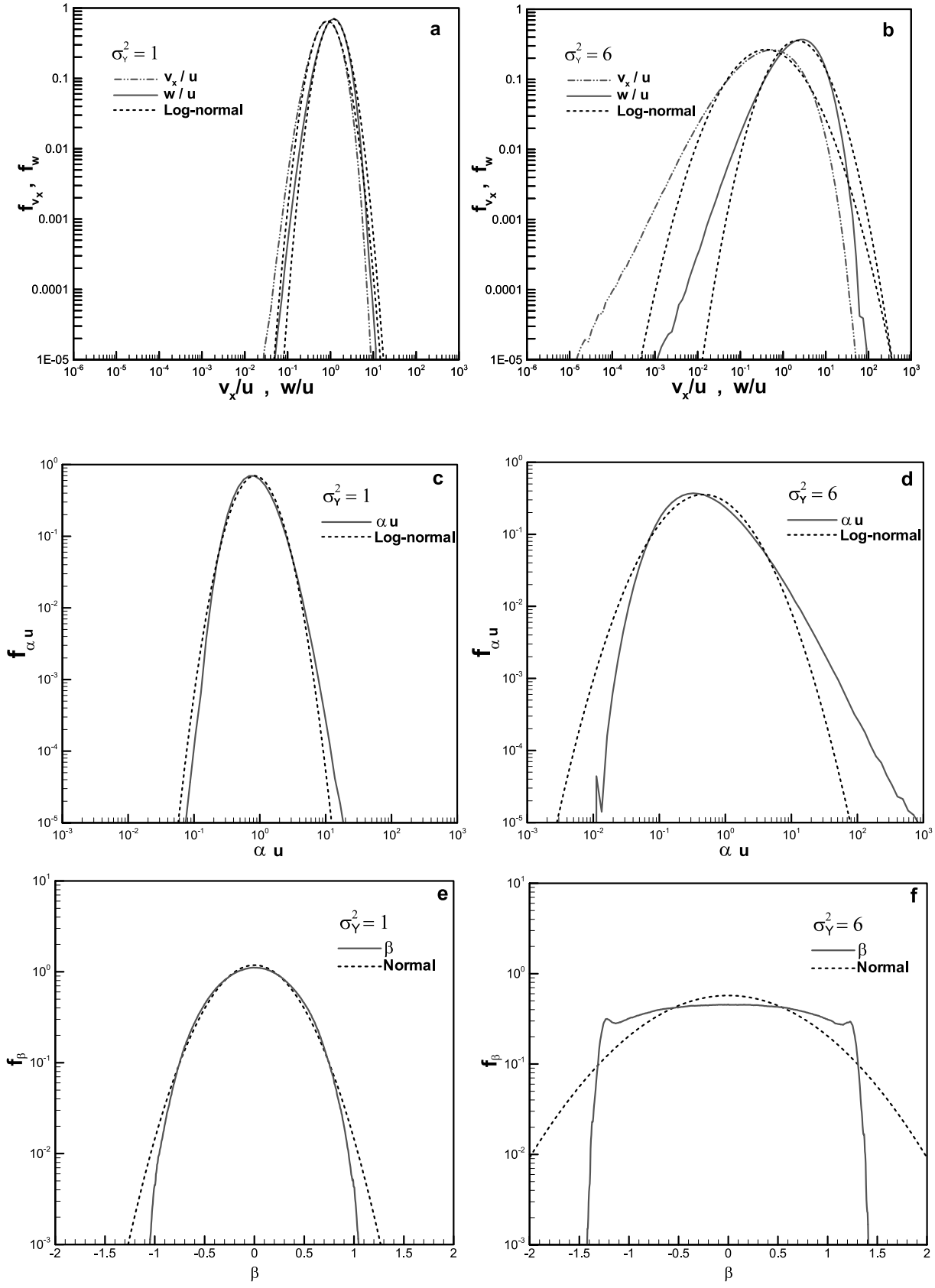

Figure 9. Velocity pdf's in log-log scale: Eulerian and Langrangian velocity pdf for (a) $\sigma_Y^2 = 1$ and (b) $\sigma_Y^2 = 6$, inverse Langrangian velocity or slowness (α) pdf for (c) $\sigma_Y^2 = 1$ and (d) $\sigma_Y^2 = 6$. Comparison with lognormal distributions is also included. Pdf's of slope (β) in semilog scale for (e) $\sigma_Y^2 = 1$ and (f) $\sigma_Y^2 = 6$. Comparison with normal distributions is also included. Simulations 1–6 are used for Figures 9a–9d, and 7–8 and 10 are used for Figures 9e–9f.

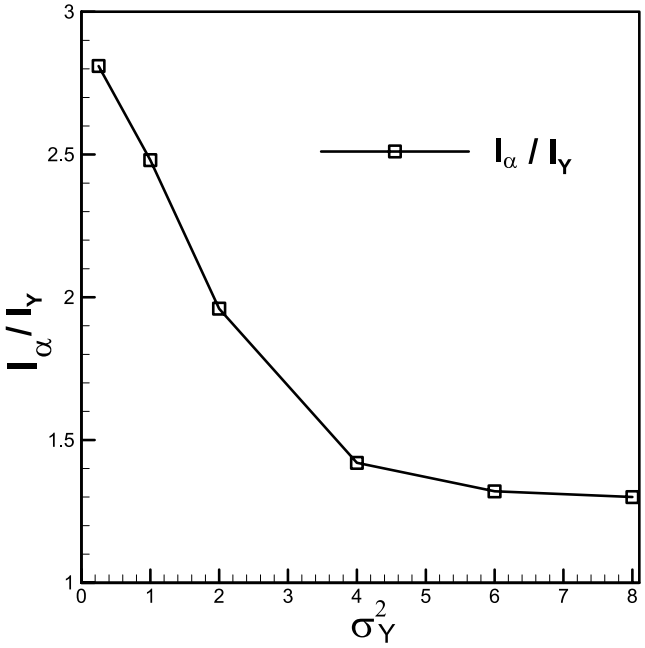

Figure 10. Integral scale of the slowness (α) as a function of σ_Y^2. Simulations 1–6 are used (Table 1).

tailings in comparison with the normal distribution. Two small peaks occur symmetrically and approximately at $\pm E(\lambda)$, representing influence of the vertical flow (and also backward flow) due to bypassing of low-conductivity zones.

7. Estimators for Asymptotic Longitudinal Dispersion

[48] From the application perspective, the main interest is predictive modeling of tracer transport, in particular the possibility of relating a few key transport quantities to measurable properties such as statistical parameters of the hydraulic conductivity. The first-order theory provides a robust predictive model for low to moderate *lnK* variances; however, its limitations for highly heterogeneous porous media are apparent for $\sigma_Y^2 > 1$.

[49] Different conceptual strategies for modeling transport in heterogeneous porous media have been presented in the literature, such as the trajectory approach [*Dagan*, 1984; *Cvetkovic and Dagan*, 1994a, 1994b], fractional diffusion equation [*Benson et al.*, 2000], nonlocal transport approaches [*Cushman and Ginn*, 1993; *Neuman and Orr*, 1993], and continuous random walk methods [*Scher et al.*, 2002; *Berkowitz et al.*, 2002]. In spite of these theoretical advances, our main problem still remains understanding the flow velocity and its Lagrangian variants (such as slowness) and their relationship with the statistics of the hydraulic conductivity. Here we shall focus our discussion on longitudinal transport as quantified by the statistics of travel time, in an attempt to provide simple and robust estimators first of the slowness statistical properties, and then of the travel time variance and the corresponding longitudinal dispersivity for highly heterogeneous media with $\sigma_Y^2 \geq 4$.

[50] Dimensionless travel time variance can be described asymptotically as

$$\frac{\sigma_\tau^2 u^2}{I_Y^2} \rightarrow 2\sigma_\alpha^2 u^2 \left(\frac{I_\alpha}{I_Y}\right)\left(\frac{x}{I_Y}\right). \tag{17}$$

We first recognize in Figure 6d that a reasonably good estimator for slowness variance is a polynomial of the form

$$\sigma_\alpha^2 u^2 = \frac{\sigma_Y^2}{4} + \frac{\sigma_Y^4}{5} + \frac{\sigma_Y^6}{500}. \tag{18}$$

Next, we compute the integral scale of I_α from correlation function in Figures 8b and 8c to obtain a relatively simple dependence of I_α on σ_Y^2. Figure 10 indicates that the slowness integral scale decreases with increasing heterogeneity variability, converging to about $(4/3)I_Y$ for $\sigma_Y^2 \geq 6$. Note that this is in contrast to what was assumed by *Cvetkovic et al.* [1996] with resident injection mode for flow and advective transport with $\sigma_Y^2 \leq 4$. As noted earlier, the decrease of I_α with an increasing level of variability can be explained by increasingly violent meandering, whereby the connectivity of slowness in the longitudinal direction also decreases.

[51] The simplest model for capturing the exponential-type curve in Figure 10 is

$$\frac{I_\alpha}{I_Y} = A + B\,\exp\left(-C\sigma_Y^4\right). \tag{19}$$

where a best estimate in least square sense is $A = 4/3$, $B = 3/2$, and $C = 1/5$.

[52] Combining the above two equations, we write equation (17) for asymptotic travel time variance in the final form

$$\frac{\sigma_\tau^2 u^2}{I_Y^2} \rightarrow 2\left(\frac{\sigma_Y^2}{4} + \frac{\sigma_Y^4}{5} + \frac{\sigma_Y^6}{500}\right)\left(\frac{4}{3} + \frac{3}{2}\exp\left(-\frac{1}{5}\sigma_Y^4\right)\right)\frac{x}{I_Y}. \tag{20}$$

Note that this asymptotic estimator is robust for high σ_Y^2 due to the near-linear dependence of travel time variance on distance only after a few integral scales (due to small correlation length of the slowness; Figures 9b and 9c). The complete linear behavior of the travel time variance and consequently asymptotic longitudinal dispersion is reached at a double distance where slowness correlation approaches approximately zero (equation (5)). Figures 8b and 8c show that after around $30I_Y$ slowness correlation reaches zero which means that after $60I_Y$ longitudinal dispersion becomes equal to the asymptotic (macrodispersion) longitudinal constant coefficient.

[53] In view of the relationship between the longitudinal dispersion coefficient and travel time variance (that is typically used in the time domain with the variance of particle position [*Dagan* [1989]),

$$\frac{\lambda_L}{I_Y} = \frac{1}{2}\frac{d\left(\sigma_\tau^2 u^2 / I_Y^2\right)}{d\left(x/I_Y\right)}, \tag{21}$$

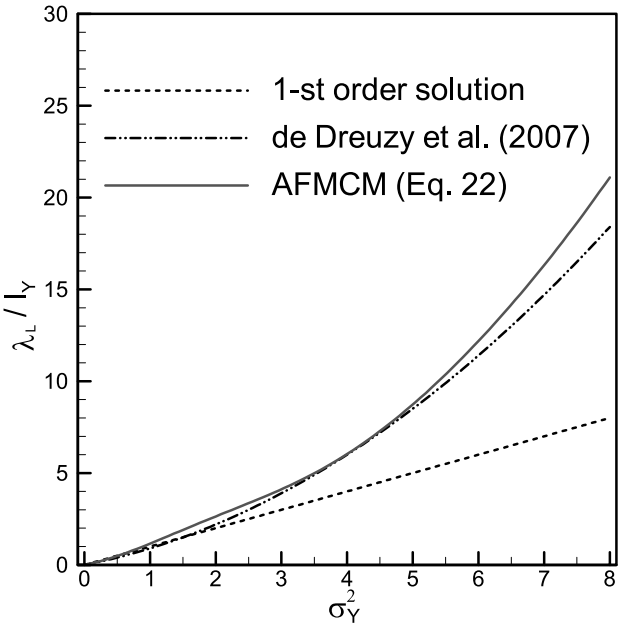

Figure 11. Asymptotic longitudinal dispersion as a function of σ_Y^2.

the longitudinal dispersivity λ_L can now be expressed in the dimensionless form combining equations (20) and (21) as

$$\frac{\lambda_L}{I_Y} = \left(\frac{\sigma_Y^2}{4} + \frac{\sigma_Y^4}{5} + \frac{\sigma_Y^6}{500}\right)\left(\frac{4}{3} + \frac{3}{2}\exp\left(-\frac{1}{5}\sigma_Y^4\right)\right). \quad (22)$$

Because of a linear dependence of σ_τ^2 with distance, in particular for increasing σ_Y^2, dimensionless longitudinal dispersivity in (22) depends only on log conductivity variance. *Salandin and Fiorotto* [1998] and *de Dreuzy et al.* [2007] presented analysis of dispersivity for 2-D case with exponential covariance, whereas *Janković et al.* [2003] and *Fiori et al.* [2006] considered dispersivity for 2-D and 3-D cases with non-Gaussian heterogeneity structures, where longitudinal dispersivity was determined as a function of time. We can directly compare equation (22) with first-order theory [*Dagan*, 1989] ($\lambda_L = \sigma_Y^2$) and recent simulations results for normalized longitudinal asymptotic effective dispersivity of *de Dreuzy et al.* [2007]; their average fitted curve $\lambda_L = 0.7\sigma_Y^2 + 0.2\sigma_Y^4$ compares reasonably with our estimator (22), especially for high heterogeneity around $\sigma_Y^2 = 4$ (Figure 11). Small deviations occur for mild heterogeneity ($\sigma_Y^2 = 1-2$) and extremely high heterogeneity (relative error for $\sigma_Y^2 = 8$ is around 14%). Furthermore, these results also agree with the recent study of *Dentz and Tartakovsky* [2008] who showed that the classic first-order theory using two-point closure scheme is insufficient for the correct calculation of the longitudinal dispersion and significantly underestimates the macrodispersion value for high heterogeneity ($\sigma_Y^2 > 4$).

[54] It is worthwhile noting that the "spatial" travel time approach can provide an asymptotic longitudinal dispersivity using a relatively small domain, in comparison with the "temporal" position approach which requires a larger domain (e.g., *Janković et al.* [2003], where hundreds of integral scales in 2-D and 3-D were used, or *de Dreuzy et al.* [2007], with 2-D simulations in an approximately $1600I_Y \times 800I_Y$ domain). For each control plane, all slow and fast streamlines are integrated and considered through the travel time distribution, covering all temporal scales; this requires long time simulations but in relatively small domains. "Temporal" concept is computationally more demanding because it requires a similar number of fast and slow streamlines and therefore a similar number of data for all lag times. However, in highly heterogeneous porous media there are only few percent of slow streamlines (reflected by the tail of the travel time pdf, Figure 4) and displacement statistics for large times exhibit significant fluctuations and uncertainties. Therefore particle position analysis requires large domains and number of streamlines to include all time lags and enable reliable statistics [*de Dreuzy et al.*, 2007].

[55] To test equation (22) and assess the nature of the dispersion process, we shall use the mean and variance of travel time (20) in the inverse Gaussian model defined by

$$f_\tau = \frac{1}{\sqrt{2\pi\,\sigma_\tau^2(\tau/\overline{\tau})^3}}\exp\left(-\frac{(\tau-\overline{\tau})^2}{2\,\sigma_\tau^2\tau/\overline{\tau}}\right). \quad (23)$$

Equation (23) is the solution of the advection-dispersion equation for a semi-infinite domain and injection in the flux [*Kreft and Zuber*, 1978]. A comparison is made for different variances σ_Y^2 at a few selected distances in Figures 12a–12d.

[56] From low to moderate variability ($\sigma_Y^2 \leq 3$), inverse Gaussian pdf reproduces reasonably well the actual pdf (Figure 12a) in particular for $x/I_Y \geq 10$. For high heterogeneity ($\sigma_Y^2 > 3$) and small distances from the source area ($x/I_Y \leq 20$), inverse Gaussian pdf deviates from the simulated pdf in the first part of the breakthrough curve. However, with increasing distance, the difference between simulated and modeled curves decreases, while after around $40I_Y$ the inverse Gaussian pdf reproduces well the peak and later part of the experimental pdf (Figures 12b–12d). A second set of simulations with larger longitudinal domain of $100I_Y$ shows similar deviations between the actual travel time pdf and ADE approximation. We observe that transport in highly heterogeneous porous media is non-Fickian for the first $40I_Y$ ($100I_Y$). Qualitatively, ADE solution as well as lognormal distribution cannot fully reproduce the features of the simulated travel time pdf in highly heterogeneous porous media. We therefore conclude that the first two moments are not sufficient for a complete description of the travel time distribution for high σ_Y^2 and distances up to $40I_Y$ ($100I_Y$) [e.g., *Bellin et al.*, 1992; *Cvetkovic et al.*, 1996; *Woodbury and Rubin*, 2000].

8. Preasymptotic Behavior of the Transverse Dispersion

[57] Transverse dispersion was analyzed with respect to the first-order theory [e.g., *Dagan*, 1989], second-order theory [*Hsu et al.*, 1996], numerical simulations in multi-Gaussian formations for low and high heterogeneity [*Salandin and Fiorotto*, 1998; *de Dreuzy et al.*, 2007], or recently in non-Gaussian highly heterogeneous fields [*Janković et al.*, 2003]. These analyses presented that transverse dispersion in 2-D fields for pure advection

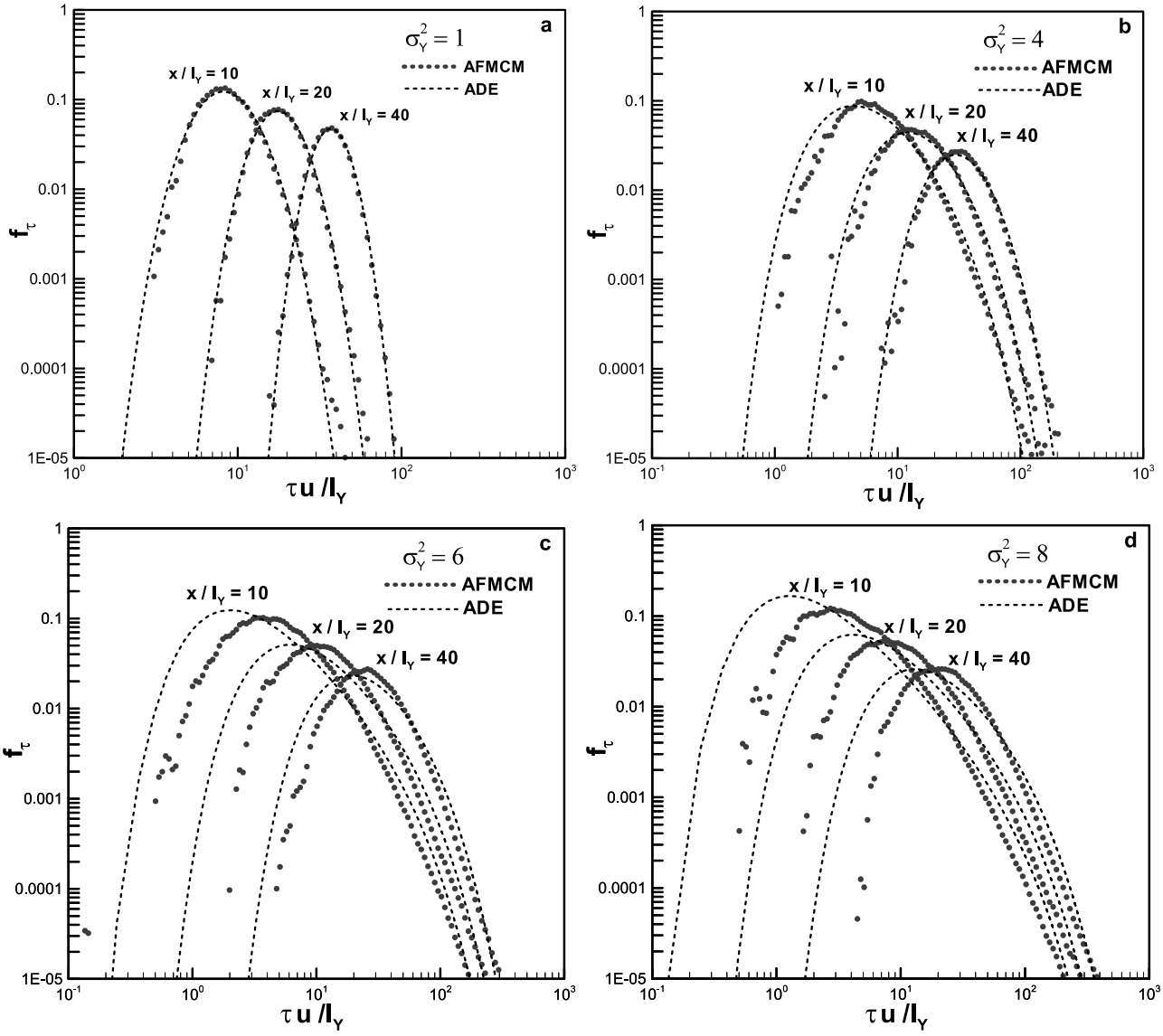

Figure 12. Comparison between actual AFMCM travel time pdf and inverse Gaussian pdf (ADE solution) for three different control planes and four considered σ_Y^2 in log-log scale: (a) $\sigma_Y^2 = 1$, (b) $\sigma_Y^2 = 4$, (c) $\sigma_Y^2 = 6$, and (d) $\sigma_Y^2 = 8$. Simulations 1–6 are used for all cases (Table 1).

increases in time until it rapidly reaches a maximum value and then slowly decreases to zero. This behavior was proved for low as well as high heterogeneity [*de Dreuzy et al.*, 2007]. A convenient measure of transverse dispersivity can be obtained from the second transverse displacement moment (σ_η^2) in analogy with the longitudinal dispersivity (equation (21))

$$\frac{\lambda_T}{I_Y} = \frac{1}{2}\frac{d\left(\sigma_\eta^2/I_Y^2\right)}{d\left(x/I_Y\right)}. \tag{24}$$

Letting $x/I_Y \rightarrow \infty$ and using equation (5), equation (24) transforms to the following asymptotic form:

$$\frac{\lambda_T}{I_Y} = \sigma_\beta^2\left(\frac{I_\beta}{I_Y}\right). \tag{25}$$

Therefore asymptotic transverse dispersion depends only on the second moment of the slope function, more precisely, on its variance and integral scale. Figure 8d shows that integral scale of the slope function converges to the zero, which means that transverse macrodispersion value also goes to zero as in the "temporal" Lagrangian approach. However, we can show only preasymptotic behavior because asymptotic distance outperforms our current computational capacity. Figure 13 presents preasymptotic behavior of the transverse dispersion (domain $128I_Y \times 64I_Y$) within the first $60I_Y$ in which maximum value is reached after only $4-5I_Y$, followed by a decreases for $\sigma_Y^2 \geq 4$, but with a slower rate for increasing σ_Y^2.

9. Discussion

[58] The most important consequence of the high heterogeneity is changing the flow patterns in the form of

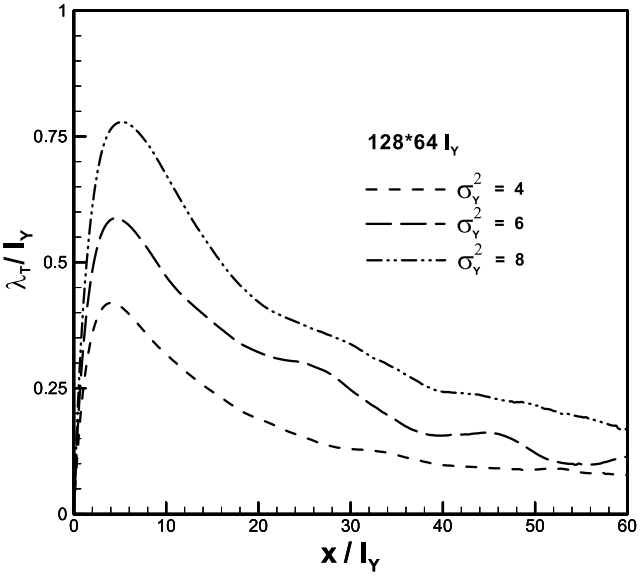

Figure 13. Preasymptotic transverse dispersion for high heterogeneity as a function of x/I_Y. Simulations 7–8 and 10 are used (Table 1).

preferential flow channels, which is reflected by a significant difference between Eulerian and Lagrangian velocities (Figures 9a and 9b). Preferential flow channels connect highly conductive zones and concentrate the main portion of the flow rate to few flow paths. Therefore Lagrangian velocity records the higher values, in contrast to the Eulerian velocity which contains a significantly larger fraction of low velocities [*Cvetkovic et al.*, 1996]. Both pdf's exhibit strongly nonlognormal behavior.

[59] High heterogeneity also introduces significant changes to the correlation structure of all Eulerian and Lagrangian flow variables (v_x, v_y, w, α, and β). For example, v_x, w, and α have essentially the same correlation structure for low heterogeneity. High heterogeneity affects strongly the correlation structure for v_x, w, and α due to increasingly dramatic meandering and consequently decreases correlation length and integral scale, except for the Lagrangian velocity w, which attains a nonzero correlation over many log conductivity integral scales due to persistency of channeling. On the other side, v_y and β shows the "hole effect" and its integral scale in the longitudinal direction converges to the zero. This paper focuses on the second moment of advective transport with respect to the covariance of slowness and slope which completely determines travel time and transverse displacement variances by equation (5) which in turn completely defines longitudinal (equation (21)) and transverse dispersion (equation (24)) as common measures of plume spreading (ADE). Furthermore, correlation of the slowness and slope as well as its integral scales determines asymptotic dispersion behavior and plays a key role in the advective transport as quantified by the travel time approach [*Dagan et al.*, 1992].

[60] Travel time variance results of the present study with in-flux injection, and those of *Cvetkovic et al.* [1996] with resident injection, expose a very important influence of the injection mode to the advective transport [*Demmy et al.*, 1999]. In the flux injection mode, initial Lagrangian velocity distribution is the flux weighted Eulerian velocity pdf, which is equal to the asymptotic Lagrangian velocity pdf [*Le Borgne et al.*, 2007]. It means that Lagrangian velocity pdf is the same at each control plane, which implies that Lagrangian velocity, as well as slowness and slope, is statistically stationary with constant mean and variance, while correlation depends only on separation distance (section 6).

[61] Contrarily, resident injection mode exhibits nonstationarity of Lagrangian velocity close to the source line since it transforms from initially Eulerian velocity distribution to the asymptotic Lagrangian distribution. *Le Borgne et al.* [2007] proved that in multi-Gaussian fields after around $100I_Y$ (practically around $20I_Y$), particles "loose memory" of the initial velocity, which means that in both injection cases an asymptotic Lagrangian velocity distribution is equal to the flux-weighted Eulerian velocity pdf and does not depend on the injection mode. *Demmy et al.* [1999] showed that travel time deviations between different modes occur even for $\sigma_Y^2 < 1$, while *Cvetkovic et al.* [1996] showed that for high heterogeneity ($\sigma_Y^2 > 3$) travel time variance changes from the concave to the convex form increasing considerably values within the first $7-12I_Y$, after which a similar slope as for the variance in the flux injection mode is exhibited (compare their Figure 7 and our Figure 3). This preasymptotic behavior is closely related to the velocity conditional correlation of *Le Borgne et al.* [2007] because many particles injected in low-conductivity zones require sufficient distance to reach preferential flow channels which carry a large part of the plume. Therefore longitudinal dispersion in resident injection mode rapidly increases within the first $7-12I_Y$, reaching the maximum value that is higher than the asymptotic value, and then gradually decreases to the asymptotic value estimated by equation (22).

[62] Most related studies (including this work) discuss flow and transport in multi-Gaussian heterogeneity structures which are completely characterized by first two moments and lack of correlation for low and high conductivity values. Many field experiments show that multi-Gaussian field may not be realistic, mainly due to neglecting significant correlation of highly connected zones (e.g., MADE-1 and MADE-2 tracer test [*Boggs et al.*, 1992]). Moreover, differences between multi-Gaussian and some selected non-Gaussian fields are discussed with respect to the travel time [*Gomez-Hernandez and Wen*, 1998], macrodispersion [*Wen and Gomez-Hernandez*, 1998], mass transfer [*Zinn and Harvey*, 2003], and especially influence of the highly connected conductivity zones on flow and transport analysis [*Zinn and Harvey*, 2003; *Liu et al.*, 2004; *Knudby and Carrera*, 2005]. Particularly, *Gomez-Hernandez and Wen* [1998] and *Zinn and Harvey* [2003] argue that first arrivals can be 10 times faster in non-Gaussian fields which are important for risk assessment, for instance. Moreover, *Wen and Gomez-Hernandez* [1998] proved that even in a case of low heterogeneity, macrodispersion could be considerably different in non-Gaussian fields. Furthermore, presented results show asymmetry of the travel time and velocity distributions is enhanced compared with the lognormal distribution for large σ_Y^2, implying that the classical analytical first-order theory, which is based on assuming equality of Eulerian and Lagrangian velocities, is robust only for $\sigma_Y^2 < 1$, especially in the presence of arbitrary non-

Table 4. Percentage of the Negative Velocity (Backward Flow) for Eulerian and Lagrangian Velocity[a]

σ_Y^2	$p(v_x, w < 0) \times 100\%$
0.25	0
1	10^{-4}
2	0.060
4	1.411
6	2.713
8	4.819

[a]Simulations 1–10 are used.

Gaussian and highly heterogeneous fields. Thus the first two moments are insufficient, and higher moments are needed in order to reproduce the enhanced skewness of the pdf, kurtosis, and particularly prediction of the tailing.

[63] An estimator for longitudinal dispersion (22) for multi-Gaussian fields is in reasonable agreement with estimator of *de Dreuzy et al.* [2007]. Recently, *Fiori et al.* [2008] discussed arguments why their own estimator for non-Gaussian fields overestimates the one of *de Dreuzy et al.* [2007] for high heterogeneity ($\sigma_Y^2 > 6$). They put forward two main arguments: (1) different heterogeneity structure and (2) possible numerical error due to the approximation of travel time tailings [*Fiori et al.*, 2008, Figure 5]. Our Figure 4 confirms that in multi-Gaussian fields, travel time pdf tailings can be computed very accurately without significant statistical fluctuations; consequently, accurate calculations of the travel time variance can be obtained for estimator (22). Multi-Gaussian fields do not contain extremely slow streamlines which travel only in low-conductivity zones and produce very large travel times and therefore higher travel time variance and longitudinal dispersion. We can conclude that the main reason for this estimator difference between our results and *de Dreuzy et al.* [2007] on the one side, and *Fiori et al.* [2006, 2008] on the other is the difference in heterogeneity structure [*de Dreuzy et al.*, 2008].

[64] The Lagrangian theory developed for travel time analysis using the distance along the mean flow as an independent variable (x/I_Y) [*Dagan et al.*, 1992; *Cvetkovic et al.*, 1992, 1996] is strictly applicable only if the longitudinal velocity component is positive at all points such that the longitudinal displacement X(t) is monotonically increasing. In the present study, we extend the conceptual framework (section 3) consistent with Monte Carlo simulations which can accurately describe even backward flow through the control plane and found that there is an increasing fraction of negative longitudinal velocities or backward flow components for increasing σ_Y^2. The exact fractions are given in Table 4. Backward flow occurs on trajectories which bypass extremely low permeable zones. For high heterogeneity with $\sigma_Y^2 = 8$, there is almost 5% of the negative Eulerian and Lagrangian velocities.

[65] Figure 14 presents quantitative analysis of the influence of the backward flow for $\sigma_Y^2 = 6$. Figures 14a and 14b shows travel time and transverse displacement variance and perfect agreement between MC simulations and equation (5) using the covariance of the slowness and slope. This agreement proves the validity of conceptual framework, definition of the slowness and slope, and its weak stationarity. If we remove all streamline points with negative horizontal velocity from the statistics in equation (5), it is possible to calculate related variances without influence of the backward flow. Figure 14a indicates that backward flow yields around 5% higher travel time variance because trajectories bypass extremely low-conductivity zones, but on average, the Lagrangian velocities in backward flow are smaller than mean velocity which produces larger travel times and therefore larger variance. Nevertheless, influence of the backward flow is more important for the transverse displacement variance (Figure 14b), increasing it around 16% due to significant influence of the vertical component of Lagrangian velocity. Note that MC simulations record all multiple travel time passages and backward flow, but calculate only first time passages at the control plane (equations (1)–(6)). A general framework for transport analysis suitable for relating particle position and travel

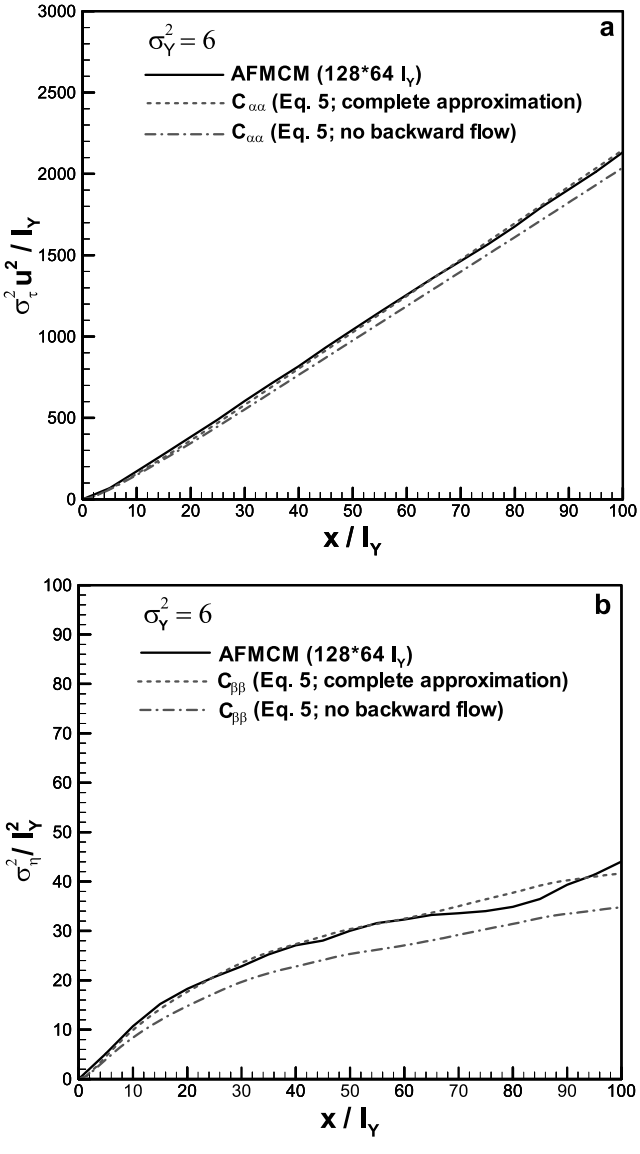

Figure 14. Influence of the backward flow for high-heterogeneity case $\sigma_Y^2 = 6$ through (a) travel time variance obtained by AFMCM (domain $128I_Y \times 64I_Y$) and covariance of the slowness function (b) transverse displacement variance obtained by AFMCM (domain $128I_Y \times 64I_Y$) and covariance of the Lagrangian slope function.

time pdfs with multiple crossings is the continuous time random walk method [*Berkowitz et al.*, 2002; *Scher et al.*, 2002], which could be used for further studies of backward flow effects.

[66] This work clearly emphasizes the need for further scrutiny of the early arrival times. The simulated travel time pdf's exhibit the tendency of delayed first arrival compared with the lognormal and inverse-Gaussian distributions, a behavior that in part is due to a limited number of realizations. An earlier arrival as predicted by the two-parameter models considered (ADE and lognormal) is conservative from, say, a risk assessment perspective; however, the overestimation may be rather extreme when considering strongly decaying contaminants. In such cases, a relatively small difference in early arrival may result in dramatic differences in the peaks. Thus there is a need from both theoretical and application perspectives to gain a better understanding on how to accurately model early arrival [*Margolin and Berkowitz*, 2004]; one interesting possibility is to consider joint space, time, and velocity statistics in a random walk model [*Le Borgne et al.*, 2008]. The key challenge for applications is to relate in an effective way early arrival statistics to structural properties of the *lnK* field.

10. Conclusions

[67] In this paper we present flow and travel time ensemble statistics based on a new simulation methodology (AFMCM) which was developed by *Gotovac et al.* [2009]. As a benchmark case, a two-dimensional, steady flow, and advective transport was considered in a rectangular domain characterized by multi-Gaussian heterogeneity structure with an isotropic exponential correlation and *lnK* variance σ_Y^2 up to 8. Lagrangian transport was analyzed using travel time and transverse displacement statistics given as functions of the longitudinal distance x [e.g., *Shapiro and Cvetkovic*, 1988; *Cvetkovic et al.*, 1996]. Moreover, in-flux injection mode is considered [*Demmy et al.*, 1999].

[68] The main conclusions of this work can be summarized as follows:

[69] 1. Results confirm earlier findings for flow and travel time statistics for $\sigma_Y^2 < 4$, indicating the first-order model is robust for $\sigma_Y^2 \leq 1$; for larger σ_Y^2 we find a few new features.

[70] 2. Even for high σ_Y^2, the transverse displacement variance retains the form predicted by the first-order results, but with significant underestimation of the first-order model prediction.

[71] 3. Travel time variance exhibits an almost perfectly linear dependence with distance for high σ_Y^2, but with values several times higher than predicted by first-order expressions; this suggests a relatively simple relationship for estimating a constant longitudinal dispersivity, λ_L (equation (22)).

[72] 4. The Lagrangian and Eulerian velocity statistics and correlation functions diverge for increasing σ_Y^2 due to channelized flow, with the pdf of w shifted to the higher values and with increasing/more persistent correlation. Both pdf's are strongly nonlognormal for high heterogeneity, while asymptotic Lagrangian velocity pdf is equal as a flux-averaged Eulerian velocity distribution.

[73] 5. Pdf of η is non-Gaussian for all σ_Y^2 and control planes close to the injection source line with higher portion of zero values. However, distribution of η seems to converge to a Gaussian distribution even for high σ_Y^2 after $x/I_Y = 20$ (Table 3).

[74] 6. Pdf of τ was found to be asymptotically power law with lowest exponent being 1:3 for $x = 10I_Y$ and $\sigma_Y^2 = 8$; the slopes increase (become steeper) for increasing distance. Comparison of the experimental pdf with inverse Gaussian pdf (ADE solution) in a semi-infinite domain as well as with lognormal distribution shows that transport in highly heterogeneous porous media may deviate from these models for the first $40(100)I_Y$, in particular, regarding the first arrivals. Thus the first two moments are insufficient for complete description of travel time arrivals, peak, and tailings.

[75] 7. Correlation of slowness decreases with increasing σ_Y^2 implying that after $60I_Y$ travel time variance attains a linear shape and reaches asymptotic longitudinal dispersion estimated by equation (22); correlation of slope exhibits a "hole effect" with integral scale converging to zero which appears that the asymptotic transverse dispersion converges to zero as predicted by *de Dreuzy et al.* [2007].

[76] There are a number of open issues, the resolution of which may take advantage of the proposed AFMCM approach. Larger domains, as well as three-dimensional domains, could be studied with a comparable accuracy as in this study, if, say, Gaussian covariance structure for *lnK* is assumed, rather than an exponential one. Another important topic is incorporating pore-scale dispersion in the simulations where the semianalytical basis of the AFMCM may offer several advantages for incorporating, say, random (Brownian) steps between streamline; in particular, the derivative $\partial\eta(x;a)/\partial a$, where a is the initial location, quantifies the relative distance between streamlines important for establishing criteria for random steps. The statistics of α and β presented in this work can be a starting point for constructing random walk models for longitudinal and transversal dispersion in high heterogeneous media; to this end, a better understanding on how to define relevant steps/segments is of interest, as well as the relevance of segment to segment correlation [e.g., *Painter et al.*, 2008]. Finally, we emphasize the need to further study early particle arrival in highly heterogeneous porous media. To this end, one viable approach would be the derivation of higher-order moments using AFMCM and a reconstruction of the pdf by means of the maximum entropy principle [*Christakos*, 2000]; such analysis is currently in progress.

Appendix A: Inner Computational Domain for Transport Simulations

[77] Figure 1 shows a 2-D computational domain for steady state and unidirectional flow simulations using three sets of simulations defined on domains $64I_Y \times 32I_Y$ ($n_Y = 8$ collocation points per integral scale, $n_h = 32$), $128I_Y \times 64I_Y$ ($n_Y = 4$, $n_h = 16$), and $64I_Y \times 128I_Y$ ($n_Y = 4$, $n_h = 16$) with 500 MC realizations (Table 1). These resolutions are selected according to the accuracy and convergence analysis of *Gotovac et al.* [2009]. In each flow realization there are around 2.1×10^6 head unknowns that present our current computational limit.

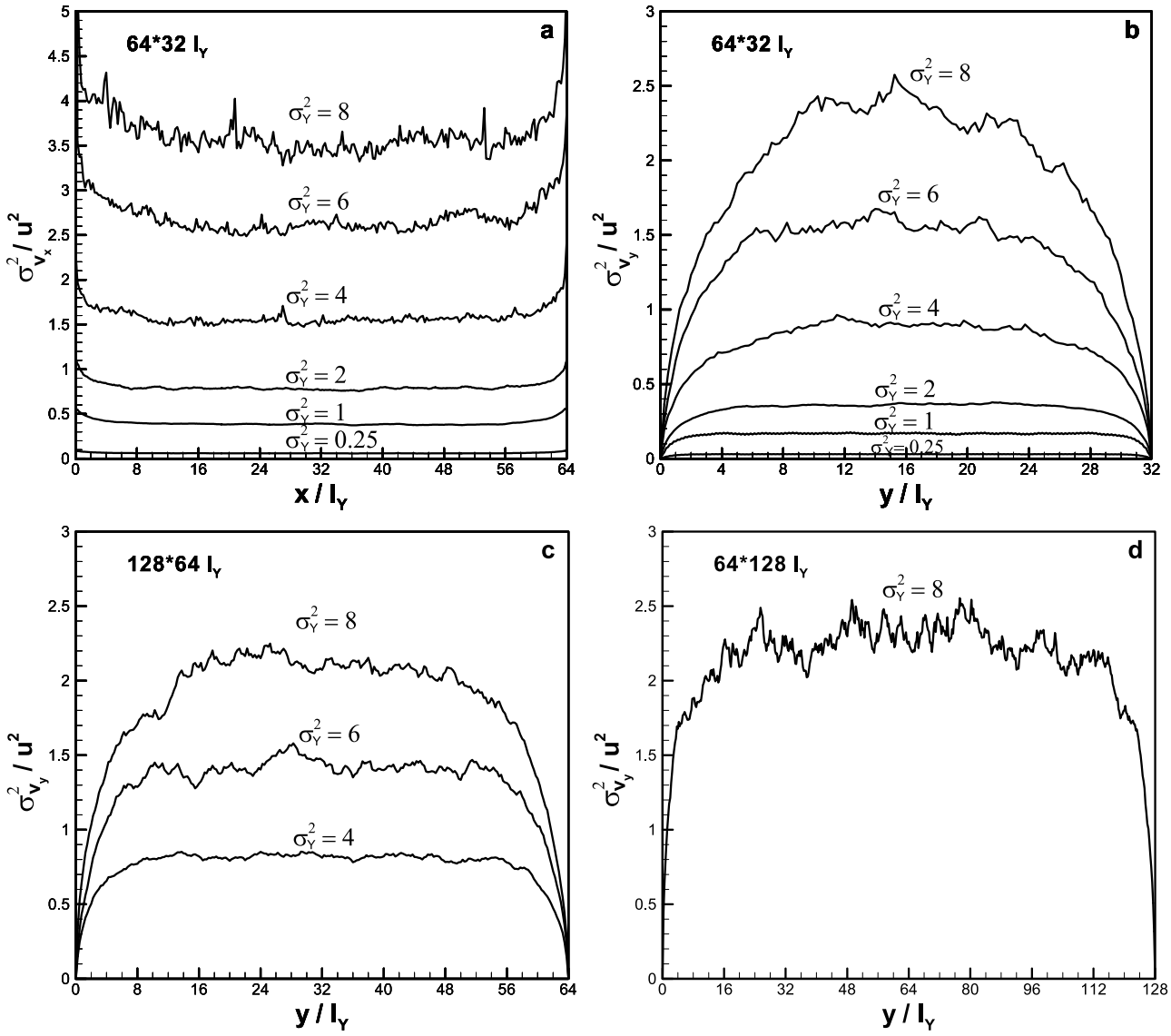

Figure A1. Influence of the flow boundary conditions presented through (a) longitudinal velocity variance along x direction for domain $64I_Y \times 32I_Y$, (b) transverse velocity variance along y direction for domain $64I_Y \times 32I_Y$, (c) transverse velocity variance along y direction for domain $128I_Y \times 64I_Y$, and (d) transverse velocity variance along y direction for domain $64I_Y \times 128I_Y$, for different σ_Y^2, $n_Y = 4$, and $n_h = 16$ (simulations 1–10; see Table 1).

[78] The influence of the boundary conditions on the nonstationarity of the Eulerian velocity statistics in case of low and mild heterogeneity was studied by *Rubin and Dagan* [1988, 1989] analytically and *Bellin et al.* [1992] numerically. Both of these studies concluded that flow criterion says that an inner computational domain should be removed at least $2-3I_Y$ from the no-flow and constant head boundaries in order to ensure stationary Eulerian velocity statistics (e.g., constant velocity variance). *Salandin and Fiorotto* [1998] and *Janković et al.* [2003] performed the same analysis in case of high heterogeneity, where typically more than $10I_Y$ were used (Figure 1). Following these works, we perform a similar analysis using AFMCM and present the results in Figure A1. We can conclude that the inner longitudinal domain should be removed by $12-14I_Y$ from the constant head boundaries in order to obtain constant longitudinal variance (Figure A1a). Transverse Eulerian velocity variance along the transversal direction is presented for all three used domains (Figures A1b–A1d). The inner transversal domain should be removed by $10-16I_Y$ from the no-flow boundaries, while this distance increases for increasing of the transversal domain. Note that all three domains yield similar Eulerian flow statistics.

[79] Transport simulations are performed in the inner domain in order to avoid nonstationary influence of the flow boundary conditions. Source area (or line, y_0) is located in the middle of the left side of the inner domain. Therefore we define transport criterion that there are no streamlines injected in the specified source line which exit

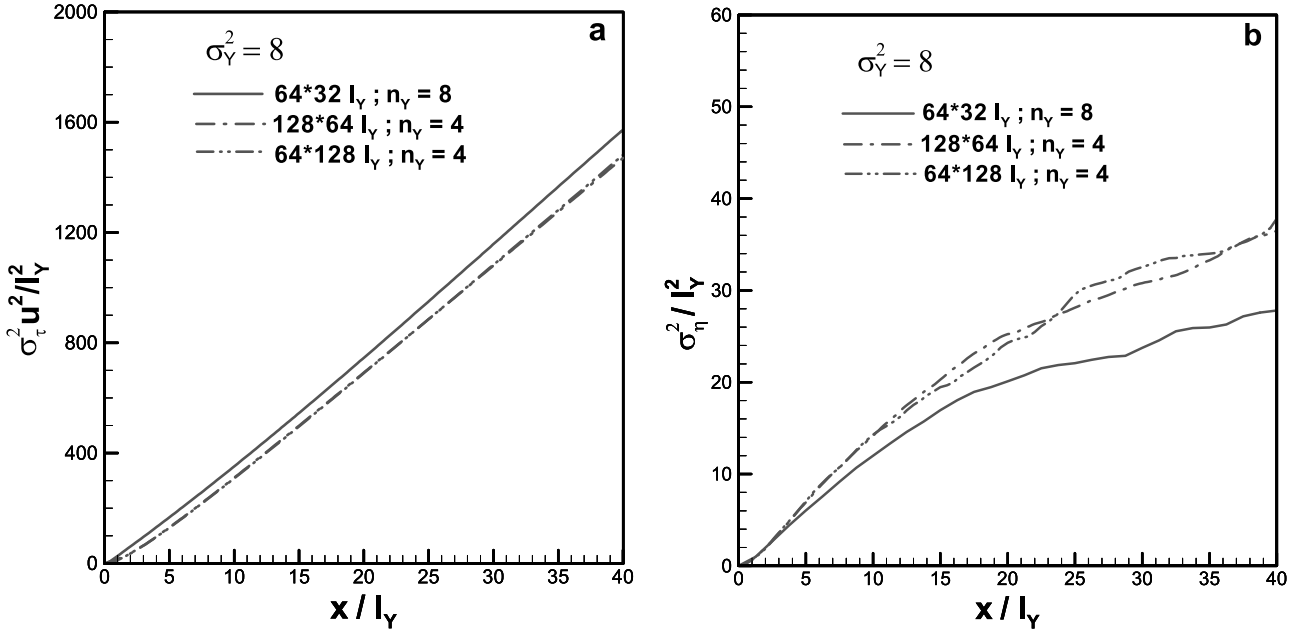

Figure A2. (a) Travel time and (b) transverse displacement variance for $\sigma_Y^2 = 8$, different domains ($64I_Y \times 32I_Y$, $128I_Y \times 64I_Y$, and $64I_Y \times 128I_Y$) and different *lnK* resolutions $n_Y = 4$ and 8 (simulations 6, 9, and 10; see Table 1).

from the inner domain. Since section 5, Figure 5, and Table 3 present that transverse displacement is nearly normal for $x/I_Y > 20$, transport criterion in transverse direction can be presented as (Figure 1)

$$y_0 + 2\, y_{\max} = y_0 + 6\sigma_\eta(x_{inner}) \le y_{inner}. \qquad \text{(A1)}$$

Figure A2 presents travel time and transverse displacement variance for $\sigma_Y^2 = 8$ and all three sets of simulations. All three domains yield comparable travel time variances, while differences occur only due to different *lnK* resolutions (Figure A2a). On the other side, transverse displacement for a domain $64I_Y \times 32I_Y$ is affected by boundaries because variance is 30% smaller than in the other two cases (Figure A2b). Therefore flow and transport criteria define that flow domain $64I_Y \times 32I_Y$ and corresponding inner domain $40I_Y \times 24I_Y$ for $\sigma_Y^2 \le 2$, flow domain $128I_Y \times 64I_Y$ and inner domain $100I_Y \times 52I_Y$ for $\sigma_Y^2 = 4$ and $100I_Y \times 46I_Y$ for $\sigma_Y^2 = 6$, and flow domain $64I_Y \times 128I_Y$ and inner domain $40I_Y \times 96I_Y$ for $\sigma_Y^2 = 8$ enable consistent flow and transport analysis free of any boundary influence, although longitudinal flow and travel time results are the same for all domains (see Table 1). According to the criterion (A1), Figure A3 shows that $y_0 = 12I_Y$ is sufficiently large to yield a travel time variance independent of the source size.

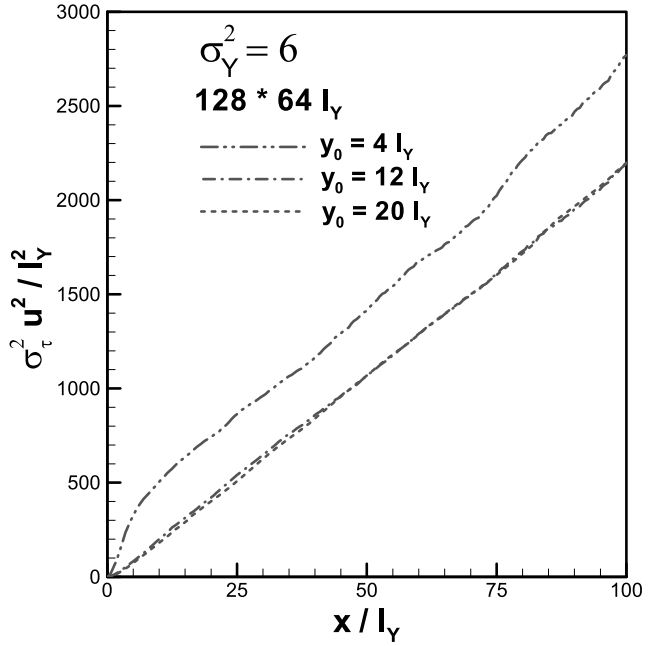

Figure A3. Travel time variance for domain $128I_Y \times 64I_Y$, $\sigma_Y^2 = 6$ and different injection sizes. Simulation 8 is used (Table 1).

[80] **Acknowledgments.** The authors wish to thank the Parallel Data Center staff at KTH-NADA (Stockholm, Sweden) for valuable help during this work. We thank J. R. de Dreuzy for velocity variance results and K.-C. Hsu for the second-order results of velocity statistics. Comments and criticism from anonymous reviewers led to improvements in this work.

References

Andricevic, R., and V. Cvetkovic (1998), Relative dispersion for solute flux in aquifers, *J. Fluid Mech.*, *361*, 145–174, doi:10.1017/S0022112098008751.

Bellin, A., and Y. Rubin (1996), HYDRO_GEN: A spatially distributed random field generator for correlated properties, *Stochast. Hydrol. Hydraul.*, *10*(4), 253–278, doi:10.1007/BF01581869.

Bellin, A., P. Salandin, and A. Rinaldo (1992), Simulation of dispersion in heterogeneous porous formations: Statistics, first-order theories, convergence of computations, *Water Resour. Res.*, *28*(9), 2211–2227, doi:10.1029/92WR00578.

Bellin, A., Y. Rubin, and A. Rinaldo (1994), Eulerian-Lagrangian approach for modeling of flow and transport in heterogeneous geological formations, *Water Resour. Res.*, *30*(11), 2913–2924, doi:10.1029/94WR01489.

Benson, D. A., S. W. Wheatcraft, and M. M. Meerschaert (2000), The fractional-order governing equation of Levy motion, *Water Resour. Res.*, *36*, 1413–1423, doi:10.1029/2000WR900032.

Berkowitz, B., J. Klafter, R. Metzler, and H. Scher (2002), Physical pictures of transport in heterogeneous media: Advection-dispersion, random-walk, and fractional derivative formulations, *Water Resour. Res.*, *38*(10), 1191, doi:10.1029/2001WR001030.

Boggs, J. M., S. C. Young, L. M. Beard, L. W. Gelhar, K. R. Rehfeldt, and E. E. Adams (1992), Field study of dispersion in a heterogeneous aquifer: 1. Overview and site description, *Water Resour. Res.*, *28*(12), 3281–3291, doi:10.1029/92WR01756.

Chin, D. A., and T. Wang (1992), An investigation of the validity of first-order stochastic dispersion theories in isotropic porous media, *Water Resour. Res.*, *28*(6), 1531–1542, doi:10.1029/92WR00666.

Christakos, G. (2000), *Modern Spatiotemporal Statistics*, Oxford Univ. Press, New York.

Cordes, C., and W. Kinzelbach (1992), Continuous groundwater velocity fields and path lines in linear, bilinear, and trilinear finite elements, *Water Resour. Res.*, *28*(11), 2903–2911.

Cushman, J. H., and T. R. Ginn (1993), Nonlocal dispersion in media with continuously evolving scales of heterogeneity, *Transp. Porous Media*, *13*, 123–138, doi:10.1007/BF00613273.

Cvetkovic, V., and G. Dagan (1994a), Transport of kinetically sorbing solute by steady random velocity in heterogeneous porous formations, *J. Fluid Mech.*, *265*, 189–215, doi:10.1017/S0022112094000807.

Cvetkovic, V., and G. Dagan (1994b), Reactive transport and immiscible flow in geological media: I. Theory, *Proc. R. Soc. London, Ser. A*, *452*, 303–328.

Cvetkovic, V., and A. M. Shapiro (1990), Mass arrival of sorptive solute in heterogeneous porous media, *Water Resour. Res.*, *26*, 2057–2067.

Cvetkovic, V., A. M. Shapiro, and G. Dagan (1992), A solute-flux approach to transport in heterogeneous formations: 2. Uncertainty analysis, *Water Resour. Res.*, *28*(5), 1377–1388, doi:10.1029/91WR03085.

Cvetkovic, V., H. Cheng, and X.-H. Wen (1996), Analysis of nonlinear effects on tracer migration in heterogeneous aquifers using Lagrangian travel time statistics, *Water Resour. Res.*, *32*(6), 1670–1680, doi:10.1029/96WR00278.

Dagan, G. (1982), Stochastic modeling of groundwater flow by unconditional and conditional probabilities: 2. The solute transport, *Water Resour. Res.*, *18*, 835–848, doi:10.1029/WR018i004p00835.

Dagan, G. (1984), Solute transport in heterogeneous porous formations, *J. Fluid Mech.*, *145*, 151–177, doi:10.1017/S0022112084002858.

Dagan, G. (1989), *Flow and Transport in Porous Formations*, Springer, Berlin.

Dagan, G. (1994), The significance of heterogeneity of evolving scales to transport in porous formation, *Water Resour. Res.*, *30*(12), 3327–3336, doi:10.1029/94WR01798.

Dagan, G., V. Cvetkovic, and A. M. Shapiro (1992), A solute-flux approach to transport in heterogeneous formations: 1. The general framework, *Water Resour. Res.*, *28*(5), 1369–1376, doi:10.1029/91WR03086.

de Dreuzy, J. R., A. Beaudoin, and J. Erhel (2007), Asymptotic dispersion in 2-D heterogeneous porous media determined by parallel numerical simulations, *Water Resour. Res.*, *43*, W10439, doi:10.1029/2006WR005394.

de Dreuzy, J. R., A. Beaudoin, and J. Erhel (2008), Reply to comment by A. Fiori et al. on "Asymptotic dispersion in 2-D heterogeneous porous media determined by parallel numerical simulations," *Water Resour. Res.*, *44*, W06604, doi:10.1029/2008WR007010.

Demmy, G., S. Berglund, and W. Graham (1999), Injection mode implications for solute transport in porous media: Analysis in a stochastic Lagrangian framework, *Water Resour. Res.*, *35*(7), 1965–1974, doi:10.1029/1999WR900027.

Deng, F.-W., and J. H. Cushman (1995), On higher-order corrections to the flow velocity covariance tensor, *Water Resour. Res.*, *31*(7), 1659–1672, doi:10.1029/94WR02974.

Dentz, M., and D. M. Tartakovsky (2008), Self-consistent four-point closure for transport in steady random flows, *Phys. Rev. E*, *77*, 066307, doi:10.1103/PhysRevE.77.066307.

Fiori, A., I. Janković, and G. Dagan (2006), Modeling flow and transport in highly heterogeneous three-dimensional aquifers: Ergodicity, Gaussianity, and anomalous behavior—2. Approximate semianalytical solution, *Water Resour. Res.*, *42*, W06D13, doi:10.1029/2005WR004752.

Fiori, A., I. Janković, G. Dagan, and V. Cvetkovic (2007), Ergodic transport through aquifers of non-Gaussian log conductivity distribution and occurrence of anomalous behavior, *Water Resour. Res.*, *43*, W09407, doi:10.1029/2007WR005976.

Fiori, A., G. Dagan, and I. Janković (2008), Comment on "Asymptotic dispersion in 2-D heterogeneous porous media determined by parallel numerical simulations" by J. R. de Dreuzy et al., *Water Resour. Res.*, *44*, W06603, doi:10.1029/2007WR006699.

Freeze, R. A. (1975), A stochastic conceptual analysis of one-dimensional groundwater flow in non-uniform homogeneous media, *Water Resour. Res.*, *11*, 725–741, doi:10.1029/WR011i005p00725.

Gomez-Hernandez, J. J., and X.-H. Wen (1998), To be or not to be multi-Gaussian? A reflection on stochastic hydrogeology, *Adv. Water Resour.*, *21*, 47–61, doi:10.1016/S0309-1708(96)00031-0.

Gotovac, H., R. Andricevic, B. Gotovac, V. Kozulić, and M. Vranješ (2003), An improved collocation method for solving the Henry problem, *J. Contam. Hydrol.*, *64*, 129–149, doi:10.1016/S0169-7722(02)00055-4.

Gotovac, H., R. Andricevic, and B. Gotovac (2007), Multi-resolution adaptive modeling of groundwater flow and transport problems, *Adv. Water Resour.*, *30*, 1105–1126, doi:10.1016/j.advwatres.2006.10.007.

Gotovac, H., V. Cvetkovic, and R. Andricevic (2009), Adaptive Fup multi-resolution approach to flow and advective transport in highly heterogeneous porous media: Methodology, accuracy and convergence, *Adv. Water Resour.*, *32*, 885–905, doi:10.1016/j.advwatres.2009.02.013.

Guadagnini, A., X. Sanchez-Villa, M. Riva, and M. De Simoni (2003), Mean travel time of conservative solutes in randomly unbounded domains under mean uniform flow, *Water Resour. Res.*, *39*(3), 1050, doi:10.1029/2002WR001811.

Hassan, A. E., J. H. Cushman, and J. W. Delleur (1998), A Monte Carlo assessment of Eulerian flow and transport perturbation models, *Water Resour. Res.*, *34*(5), 1143–1163, doi:10.1029/98WR00011.

Hassan, A. E., R. Andricevic, and V. Cvetkovic (2001), Computational issues in the determination of solute discharge moments and implications or comparison to analytical solutions, *Adv. Water Resour.*, *24*, 617–619, doi:10.1016/S0309-1708(00)00071-3.

Hsu, K.-C. (2004), Flow and solute transport in strongly heterogeneous porous media, *Pract. Period. Hazard. Toxic Radioactive Waste Manage.*, *8*(3), 148–154, doi:10.1061/(ASCE)1090-025X(2004)8:3(148).

Hsu, K.-C., and Y. Lamb (2000), On the second-order correction to velocity covariance for 2-D statistically isotropic porous media, *Water Resour. Res.*, *36*(1), 349–354, doi:10.1029/1999WR900298.

Hsu, K.-C., D. Zhang, and S. P. Neuman (1996), Higher-order effects on flow and transport in randomly heterogeneous porous media, *Water Resour. Res.*, *32*(3), 571–582, doi:10.1029/95WR03492.

Janković, I., A. Fiori, and G. Dagan (2003), Flow and transport in highly heterogeneous formations: 3. Numerical simulation and comparison with theoretical results, *Water Resour. Res.*, *9*(9), 1270, doi:10.1029/2002WR001721.

Janković, I., A. Fiori, and G. Dagan (2006), Modeling flow and transport in highly heterogeneous three-dimensional aquifers: Ergodicity, Gaussianity, and anomalous behavior—1. Conceptual issues and numerical simulations, *Water Resour. Res.*, *42*, W06D12, doi:10.1029/2005WR004734.

Knudby, C., and J. Carrera (2005), On the relationship between indicators of geostatistical, flow and transport connectivity, *Adv. Water Resour.*, *28*, 405–421, doi:10.1016/j.advwatres.2004.09.001.

Kreft, A., and A. Zuber (1978), On the physical meaning of the dispersion equation and its solution for different initial and boundary conditions, *Chem. Eng. Sci.*, *33*, 1471–1480, doi:10.1016/0009-2509(78)85196-3.

LeBlanc, D., S. Garabedian, K. Hess, L. Gelhar, R. Quadri, K. Stollenwerk, and W. Wood (1991), Large-scale natural gradient tracer test in sand and gravel, Cape Cod, Massachusetts: 1. Experimental design and observed tracer movement, *Water Resour. Res.*, *27*(5), 895–910, doi:10.1029/91WR00241.

Le Borgne, T., J.-R. de Dreuzy, P. Davy, and O. Bour (2007), Characterization of the velocity field organization in heterogeneous media by conditional correlation, *Water Resour. Res.*, *43*, W02419, doi:10.1029/2006WR004875.

Le Borgne, T., M. Dentz, and J. Carrera (2008), Lagrangian statistical model for transport in highly heterogeneous velocity fields, *Phys. Rev. Lett.*, *101*, 090601, doi:10.1103/PhysRevLett.101.090601.

Liu, G., C. Zheng, and S. M. Gorelick (2004), Limits of applicability of the advection-dispersion model in aquifers containing connected high-conductivity channels, *Water Resour. Res.*, *40*, W08308, doi:10.1029/2003WR002735.

Mackay, D. M., D. L. Freyberg, and P. V. Roberts (1986), A natural gradient experiment on solute transport in a sand aquifer: 1. Approach and overview of plume movement, *Water Resour. Res.*, *22*(13), 2017–2029, doi:10.1029/WR022i013p02017.

Margolin, G., and B. Berkowitz (2004), Continuous time random walks revisited: First passage time and spatial distributions, *Physica A*, *334*, 46–66, doi:10.1016/j.physa.2003.10.069.

Maxwell, R., W. E. Kastenberg, and Y. Rubin (1999), A methodology to integrate site characterization information into groundwater-driven health risk assessment, *Water Resour. Res.*, *35*(9), 2841–2855.

Moreno, L., and C. F. Tsang (1994), Flow channeling in strongly heterogeneous porous media: A numerical study, *Water Resour. Res.*, *30*(5), 1421–1430, doi:10.1029/93WR02978.

Neuman, S. P., and S. Orr (1993), Prediction of steady state flow in nonuniform geologic media by conditional moments: Exact nonlocal formalism, effective conductivity, and weak approximation, *Water Resour. Res.*, *29*(2), 341–364, doi:10.1029/92WR02062.

Painter, S., V. Cvetkovic, J. Mancillas, and O. Pensado (2008), Time domain particle tracking methods for simulating transport with retention and first-order transformation, *Water Resour. Res.*, *44*, W01406, doi:10.1029/2007WR005944.

Rubin, Y. (1990), Stochastic modeling of macrodispersion in heterogeneous porous media, *Water Resour. Res.*, *26*(1), 133–141. (Correction, *Water Resour. Res.*, *26*(10), 2631.)

Rubin, Y. (2003), *Applied Stochastic Hydrogeology*, Oxford Univ. Press, New York.

Rubin, Y., and G. Dagan (1988), Stochastic analysis of boundaries effects on head spatial variability in heterogeneous aquifers: 1. Constant head boundary, *Water Resour. Res.*, *24*(10), 1689–1697, doi:10.1029/WR024i010p01689.

Rubin, Y., and G. Dagan (1989), Stochastic analysis of boundaries effects on head spatial variability in heterogeneous aquifers: 2. Impervious boundary, *Water Resour. Res.*, *25*(4), 707–712, doi:10.1029/WR025i004p00707.

Salandin, P., and V. Fiorotto (1998), Solute transport in highly heterogeneous aquifers, *Water Resour. Res.*, *34*(5), 949–961, doi:10.1029/98WR00219.

Sanchez-Villa, X., and A. Guadagnini (2005), Travel time and trajectory moments of conservative solutes in three dimensional heterogeneous porous media under mean uniform flow, *Adv. Water Resour.*, *28*, 429–439, doi:10.1016/j.advwatres.2004.12.009.

Scher, H., G. Margolin, and B. Berkowitz (2002), Towards a unified framework for anomalous transport in heterogeneous media, *Chem. Phys.*, *284*, 349–359, doi:10.1016/S0301-0104(02)00558-X.

Shapiro, A., and V. Cvetkovic (1988), Stochastic analysis of solute arrival time in heterogeneous porous media, *Water Resour. Res.*, *24*(10), 1711–1718, doi:10.1029/WR024i010p01711.

Taylor, G. I. (1921), Diffusion by continuous movements, *Proc. London Math. Soc.*, *20*, 196–212, doi:10.1112/plms/s2-20.1.196.

Trefry, M. G., F. P. Ruan, and D. McLaughlin (2003), Numerical simulations of preasymptotic transport in heterogeneous porous media: Departures from the Gaussian limit, *Water Resour. Res.*, *39*(3), 1063, doi:10.1029/2001WR001101.

Wen, X.-H., and J. J. Gomez-Hernandez (1998), Numerical modeling of macrodispersion in heterogeneous media: A comparison of multi-Gaussian and non-multi-Gaussian models, *J. Contam. Hydrol.*, *30*, 129–156, doi:10.1016/S0169-7722(97)00035-1.

Woodbury, A., and Y. Rubin (2000), A full-Bayesian approach to parameter inference from tracer travel time moments and investigation of scale effects at the Cape Cod Experimental Site, *Water Resour. Res.*, *36*(1), 159–171, doi:10.1029/1999WR900273.

Zinn, B., and C. F. Harvey (2003), When good statistical models of aquifer heterogeneity go bad: A comparison of flow, dispersion, and mass transfer in connected and multivariate Gaussian hydraulic conductivity fields, *Water Resour. Res.*, *39*(3), 1051, doi:10.1029/2001WR001146.

R. Andricevic, Department of Civil and Architectural Engineering, University of Split, Matice hrvatske 15, 21000 Split, Croatia.

V. Cvetkovic and H. Gotovac, Department of Land and Water Resources Engineering, Royal Institute of Technology (KTH), Brinellvagen 32, SE-10044 Stockholm, Sweden. (hrvoje.gotovac@gradst.hr; gotovac@kth.se)